MECHANICS DEVELOPMENT COMPANY
927 GLENHAVEN STREET
PACIFIC PALISADES, CA. 90272

FINAL REPORT

CONTRACT NO. NAS2-7346

MEASUREMENTS OF V/STOL AIRCRAFT NOISE MECHANISMS USING PRESSURE CROSS-CORRELATION TECHNIQUES IN A REVERBERANT WIND TUNNEL

31 October 1974

W. C. Meecham and P. M. Hurdle

Submitted to:

Large Scale Aerodynamics Branch
NASA-Ames Research Center
Moffett Field, California 94035

Attention: Mr. David H. Hickey: Code FSA
M/S 247-1

TABLE OF CONTENTS

LIST OF FIGURES

ABSTRACT

A 3.8 cm. model jet is operated in a wind tunnel with cross-flow in order to determine the effect on jet noise radiated characteristics. Such cross-flow noise experiments are useful for V/STOL aircraft noise problems. In the course of the work a method was developed for the determination of noise radiating characteristics of sources within reverberant wind tunnels. The method employs cross-correlation measurements. The averaging time in the cross-correlation is determined by the amount of background noise within the wind tunnel. It is found that cross-flow increases the radiated noise by 10 dB. There was some indication of directivity, i.e., of the downstream radiation exceeding the sideline radiation.

1. INTRODUCTION

The proposed introduction of V/STOL aircraft has greatly intensified interest in noise reduction programs for aircraft. In order to meet expected government regulations it appears that there must be a 10 to 15 dB noise reduction for proposed aircraft configurations. If lift fans are to be used for the propulsion system this needed reduction poses very great problems. Similarly other power plants would require appreciable noise reduction to meet expected standards. In this report using modeling, we measure the important noise characteristics for such a high lift system. It has been found in the past that for very high Reynold's number flows (such as are customary in applications) the modeling process is reliable, i.e., the Reynold's number of the model is sufficiently large. In connection with such models, we make directional and spectral measurements of the radiated sound as a function of certain important parameters in the proposed configurations. The static pressure fluctuations within the flow are cross-correlated with the radiated sound field.

The experiments were conducted using a 3.8 cm. diameter jet supplied by air passing through a muffler (to eliminate upstream noise). The jet was located in the Ames Research Center 7'x10' tunnel and was placed with its flow perpendicular to the wind tunnel flow. (See Fig. 1.) In addition, as described in Appendix E, preliminary tests were conducted on a model jet oriented parallel to the tunnel flow. The wind tunnel was operated at relatively low flow speeds, up to Mach 0.2; the jet was run at Mach 0.62. The velocities employed yielded velocity ratios which are realistic for transitional speeds experienced in VTOL operations. A static pressure probe consisting of a B&K 0.32 cm. microphone was placed within the jet (to measure the static pressure fluctuations). A system of four far field microphones was located within the wind tunnel. (The experimental setup is described fully below.) Placing the experiment, of necessity, within the wind tunnel

means that various unwanted noises are introduced in the data. These noises consist first (and of primary importance) of the propagating noise within the wind tunnel itself. Secondly, the experimental configuration introduces self noises due to pressure fluctuations generated by the local turbulence of the flow about the far field microphones. Furthermore, we experience reverberant effects within the wind tunnel: Sound radiated by the jet, placed within the wind tunnel flow, will transmit not only directly to the far field microphones, but also by one or more reflections from the walls, to the microphones. These various unwanted sounds must be identified and removed from the data in order to obtain valid measurements. This process was accomplished primarily through the use of cross-correlation techniques, as will be described below.

2. THEORY OF NOISE PRODUCTION AND DATA PROCESSING

Meecham and Ribner [1-3] have developed a theory for the production of free-jet noise wherein the noise source is represented by the second time derivative of the static pressure within the jet. In this theory the sound field pressure is given by

$$p(\underline{x},t) = -(4\pi a_o^2)^{-1}\int_V r^{-1}\,\ddot{p}_o(\underline{y},t-r/a_o)\,d\underline{y} \qquad (1)$$

valid for subsonic turbulent flows; it should be emphasized that jets at exit usually have flow speeds well below Mach one. Moving source and hot-jet refraction effects are treated as separate problems using the sound source (1) as the basic (moving and refracting) source; a similar modeling process is common to most theories of jet noise. In (1) $p(\underline{x},t)$ is the sound field pressure observed at a position $\underline{x}$ outside the turbulent fluid at a time t, a_o is the speed of sound in the external medium and p_o is the static pressure measured within the turbulent jet at $\underline{y}$; $r = |\underline{x} - \underline{y}|$. The source is to be integrated over that volume V in which the static pressure greatly exceeds the acoustic pressure. Ordinarily this source region extends out to but a diameter or two from the axis of the turbulent jet. For subsonic flows we know that p_o is approximately equal to the pressure which would be found in an incompressible, turbulent flow. Here the $\ddot{p}_o$ is the second time derivative.

A large number of turbulent jet noise experiments have been performed by the authors and by others wherein the distant sound field pressure is cross-correlated with the static pressure (p_o) within the jet.[4-7] A relation between this correlation and the sound field intensity is obtained by multiplying (1) by p and averaging,

$$\langle p^2(\underline{x},t)\rangle = -(4\pi a_o^2)^{-1}\int_V r^{-1}\langle p(\underline{x},t)\,\ddot{p}_o(\underline{y},t-r/a_o)\rangle\,d\underline{y} \qquad (2)$$

(the sound intensity is $\langle p^2\rangle/\rho_o a_o$ where ρ_o is the air density).

Now let $D\langle p^2\rangle$ be the fraction of that quantity (proportional to the sound field intensity) which arises from the eddy of volume $D\underline{y}$ centered at $\underline{y}$, and we have

$$D\langle p^2\rangle = -(4\pi a_o^2 r)^{-1} \langle p(\underline{x},t)\, \ddot{p}_o(\underline{y}, t - r/a_o)\rangle\, D\underline{y} \qquad (3)$$

In many applications it is not practical to differentiate the static pressure as measured within the jet. It is possible to estimate the effect of this derivative by measuring the peak frequency of the spectrum of p_o, let that (angular) frequency be ω_o. Then (3) becomes approximately,

$$D\langle p^2\rangle = -(4\pi a_o^2 r)^{-1} \omega_o^2 \langle p(\underline{x},t)\, p_o(\underline{y}, t - r/a_o)\rangle\, D\underline{y} \qquad (4)$$

Many times we are interested in the sound directivity (of the eddy of volume $D\underline{y}$ centered at $\underline{y}$) when the far field microphones in different directions may be different distances, r, from the source position. To make such a comparison the equation (4) should be <u>multiplied</u> by r^2 where r is the distance from the source-eddy position to the far field position at the particular angular position in question; then ratios may be taken to determine the directivity of the source-eddy.

There is a simpler and alternative view of the measurement process which we now describe. Consider the cross correlation given in (4), the quantity which we most frequently measure; it is of course the cross correlation of the sound pressure measured at the far field position, $\underline{x}$, with the static pressure measured within the jet at the position $\underline{y}$, with r the distance between these two positions. We have the relation

$$(D\langle p^2\rangle)^{1/2} = \frac{C\, \langle p(\underline{x},t)\, p_o(\underline{y}, t - r/a_o)\rangle_m}{p_o'} \qquad (5)$$

primes indicate RMS values. The constant C is of order unity--it is discussed in Appendix A. Here $\langle\rangle_m$ refers to the maximum of the absolute value of the correlation (see Fig. 2), $D\langle p^2\rangle$ is the part of p^2 which comes from the eddy of volume $D\underline{y}$, centered at $\underline{y}$. In words, a cross correlation such as $\langle p\, p_o\rangle$ is proportional to the product of the RMS values

of the variables, i.e., sound field pressure and the static pressure. Fortunately the constant will vary little from situation to situation, so that for the determination of relative values we need not consider it.

We can use relation (5) to determine the relative sizes of sound field intensities radiated from given jet positions at given flow speeds. This we do in the data treatment of those measurements which we have made in the wind tunnel. We can obtain overall sound intensities (what would be measured in the same experiment performed in an anechoic room) by adding up (integrating) the contributions from the major contributing eddies, using the relation (5). It is understood that (5) is to be interpreted as the fraction of the overall intensity radiated from the eddy located at the position of the pressure probe measuring p_o.

An example of the processes may be useful. A sketch of a typical correlation measurement is shown in Fig. 2., plotted against a time delay τ (recalling that r is the distance from the source-eddy to the far field microphones). Here r_1 and r_2 are the distances travelled by the first and second wall reflections in going from the source-eddy or probe, position to the far field position. The reflected correlation pulses can be seen (more or less as they are found experimentally); they will be separated from the first arrival--sound travelling directly from the source position to the far field position--so long as the far field probe is more than a wavelength from the nearest wall of the tunnel. The important measurement is the maximum of the correlation function, obtained in this description by taking the value of the function at the origin. The 'noise' evident in the sketch is composed, depending on test condition, of:

a) Wind tunnel noise

b) Flow self-noise at the microphone

c) Higher order reflections of jet noise from the tunnel walls

All of these noises are uncorrelated (for small values of r) with the main pulse from the jet--which is what we want to measure.

The question of the signal-to-noise in these correlations, deserves further discussion; it can be improved by taking longer averaging times in the construction of the correlations. If the averaging time is T, then the signal-to-noise is proportional to $\sqrt{T}$. To improve the ratio by a factor of 2 we must average 4 times as long, etc. In our applications, to be described below, our signal was not always as large, compared with the noise, as desirable; within the scope of the present contract we were not able to average the correlations over sufficient time to make it so. For the measurements reported here, taken mainly within the 7'x10' wind tunnel, the main noise encountered was a set of relatively pure notes originating within the tunnel; these noises may have been whistles, which we were unable to remove within the scope of this work. However we conclude that in future work it would probably be possible to remove these unwanted sounds; that should be done for further acoustic applications within the tunnel. Without these sounds our signal to noise would have been significantly improved.

In earlier reports on this contract, we have described another method for the measurement of sound intensity and directivity within a wind tunnel. Because of the already mentioned high noise background within the tunnel, we were unable to employ this method for this work. For future reference this approach is described in Appendix B.

3. PERPENDICULAR JET

The main emphasis of this study was to identify the major noise generating regions when a model jet is subjected to a cross-flow. The following section describes the experiment and the results when a model jet is oriented normal to the flow, in a wind tunnel.

3.1 Experiment

A circular jet was aligned 90° to the flow of the 7'x10' wind tunnel at NASA Ames Research Center. The jet nozzle had a diameter of 3.8 cm. The jet exhausted from an airfoil. The basic test geometry is shown in Fig. 3. It consists of four far field microphones (B&K 1.3 cm.) condenser transducers equipped with nose cones. These microphones were located 40 jet diameters from the jet exit at 30° and 50° on either side of the static jet centerline. The static jet centerline refers to the centerline of the jet when there is zero flow in the wind tunnel. The model jet and the four far field microphones were located on the centerline of the wind tunnel.

A pressure probe (B&K 0.32 cm. condenser microphone with nose cone) was employed to measure and record the static pressure fluctuation within the turbulent volume of the jet.

The muffler described in Appendix D was used to insure that the noise generated by the jet was aerodynamic noise.

The model jet was operated at one constant speed, Mach 0.62, while the wind tunnel speed was varied. As in the case of the parallel jet the following tunnel conditions were employed:

a. Static case, no flow, Q (dynamic pressure) equal zero resulting in a velocity ratio (V_{oo}/V_j) equal zero.
b. Q equal 19 (38.4 m/sec) for a velocity ratio of 0.18.
c. Q equal 47 (60.4 m/sec) for a velocity ratio of 0.28.

In the presence of flow in the tunnel, the plume of the jet will bend in the direction of the flow. From the work of R.J. Margason[7] the jet centerline was calculated for the above two velocity ratios. These are plotted in Fig. 3

In order to compare the results of the experiment, for the two velocity ratios (0.18 and 0.28), with the static case, it was necessary that the pressure probe always be located with respect to the centerline of the model jet; further the probe axis was made parallel to this jet axis. For example if for the static case the probe was located at X/D equals 5.5 and Y/D and Z/D, then for a velocity ratio of 0.18 the probe would have to be located at X/D equals 5.3, Y/D equals zero, and Z/D equals 1.2 with the probe aligned at 34^{o} with respect to the static centerline. The coordinate system employed for the static pressure probe is shown in Fig. 4 , where the X-axis initially coincides with the jet static centerline; δ is the angle between this line and a line tangent to the bent jet centerline at a particular poin on the bent line. Therefore the angle δ is continuously changing and eventually downstream reaches a value of 90^{o}, when the wake is parallel to the tunnel flow. The coordinate axis R in Fig. 4 is a line in the X-Z plane which is at right angles to the bent jet centerline.

The velocity profiles at the model jet exit for the static case are shown in Fig. 5 for both the Y and Z axes. The profiles show the usual top-hat characteristics with good symmetry on either side of the centerline.

The experiment consisted of mapping the static pressure fluctuations on the Y and R axes for two centerline positions (measured along the bent centerline), recording the static pressure fluctuation signals at six pressure probe positions and at the four far field positions; all for the three different wind tunnel speeds previously described.

3.2 Analysis

The data analysis consisted of plotting the static pressure fluctuation contour, doing narrow band (50 Hz) frequency analyses of the recorded signals, and calculating the cross-correlation functions between the various probe positions and the four far field microphone positions. A block diagram of the equipment used in the analysis is shown in Fig. 6.

3.2.1 Static Pressure Fluctuation Profiles

The static pressure fluctuation profiles, for the static case (wind tunnel Q = 0) are shown in Fig. 7. For X/D equal 2.5 the pressure rises from the centerline (Y/D = 0) to a maximum in the shear region (Y/D = 0.4 to 0.5). From this point the pressure rapidly drops off since the shear region here is quite thin. The jet spreads slowly here; the 10% velocity line is only 0.75 D from the centerline.

At X/D equal 5.5 the difference between the centerline pressure and the maximum (shear layer) pressure is only about 1.5 to 2 dB compared to 5 to 6 dB for X/D = 2.5. In addition, the peak is much broader and has moved closer to the centerline. The fall off is much slower than that seen in the region of strong shear giving an indication of how the wake is spreading. For X/D equals 7.5 there no longer exists a shear-peak but rather we see a broad constant pressure area which stretches from the centerline to approximately Y/D equals 2/3. The fall off outside this region is even slower than that experienced at X/D =5.5, (as the jet continues to spread).

The curves in Fig. 8 show the static pressure fluctuation contours for a velocity ratio of 0.18. The probe position is equivalent to X/D equal 2.5 for the static case. It is interesting to note that there no longer exists a well defined pressure peak in the vicinity of Y/D equal 0.45 but rather there is fairly constant pressure area from the centerline to

Y/D equals 1.0, giving an indication that the so-called shear region (for lack of a better term) has become more significant especially when one takes into consideration the fact that the pressure levels have increased by approximately 6 dB over the static case. For the R axis the pressure levels drop off more rapidly, this position being 180° from the point where the tunnel flow makes initial contact with the jet. Still the drop-off is much slower than for the static case.

Fig. 9 shows the static pressure profiles for the centerline position equivalent to X/D equals 5.5 (for the static case) for a velocity ratio of 0.18. The peak levels are comparable to those measured for the static case but the fall-off is significantly slower; for example for Y/D equal 1.25, the static case gives a value of 142 dB while this curve shows slightly higher than 150 dB. The contours for the Y and R axes are very nearly symmetrical. Although the changes are not as drastic as that experienced in the so-called shear region, there is a definite increase in the size of the mixing region, due to the interaction between the jet and the free stream (tunnel flow).

Corresponding curves for a velocity ratio of 0.28 are shown in Figs. 10 and 11. Again there is a remarkable increase in activity in the shear region. The peak level in this region is slightly higher than those experienced for a velocity ratio of 0.18, but the curve for the Y axis falls off slightly faster for the higher velocity ratio, while on the other hand the R-axis falls off more slowly. At the position equivalent to approximately X/D equal 5.5 (Fig. 11) the levels are approximately 5 dB lower than those measured for the velocity ratio of 0.18, with the fall off being nearly the same.

Overall there does not seem to be a significant difference between a velocity ratio of 0.18 and of 0.28. However, there is a significant difference in the shear region structure when going from the static case

to either of the two velocity ratios. This is very noticeable in Fig. 12 where the static pressure fluctuation contours have been plotted (along the Y-axis) for the shear region of the jet, for all three wind tunnel conditions. We see there an increase of 7 to 10 dB within the shear layer for either cross-flow with 10 dB applying over most of the range. Using an 8th power velocity law for the sound field intensity (a 4th power pressure law) we deduce that there would be an increase of from 14 to 20 dB in the sound radiated from the shear layer with cross-flow. The corresponding changes in the mixing region, see Figs. 7, 9, and 11, are a few dB. The 14 - 20 dB change for the shear layer is consistent with the cross-correlation measurements discussed below, at least for the largest increase in cross-correlations found there. One has to integrate the effect of the sound sources throughout the shear and mixing regions in order to obtain the change in over-all sound levels. Thus the overall change is expected to be less than the maximum 14 - 20 dB effect deduced here.

The directivity of the sound radiated by the jet in wind-tunnel cross-flow has proved to be a particularly difficult measurement problem. The data obtained in these experiments would require more processing in order to yield really reliable results. Nevertheless, we can make some deductions concerning such sound directivity. First, referring to Fig. 3, it is seen that with either one of the cross-flows, all of our far field microphones lie on one side of the jet. They range from largest angles at microphone 1 to smallest at microphone 4. For maximum directivity effects with flow compare the results for those microphones. Looking then to the higher cross-flow speed for the shear regions in Figs. 17 and 18 (the errors shown there by flags) we note that there is little directivity effect for eddies within the shear layer. (There is a <u>possible</u> 5 dB effect--greater sound downstream--shown in Fig. 17.) Thus the shear region appears to radiate more or less isotropically. It is seen that all of these levels are, within experimental error, about (relative) 25 dB. Turning now to Figs. 19 and 20 for the mixing region (X/D = 5.5) we

see, comparing positions 1 and 4 that we might deduce up to a 5 dB decrease as the angle of observation is increased. This compares favorably with the results for a jet located at an anechoic room where the mixing region dominates. However, note again that with cross-flow the shear region, perhaps isotropic, dominates the sound from the mixing region, reducing the effect of mixing region directivity. Thus--but subject, at this stage to experimental error--we may conclude a directivity effect of no more than 5 dB, where the jet in cross-flow radiates more sound downstream than it does upstream. The corresponding determination in Ref. 9 seems somewhat ambiguous.

3.2.2. Frequency Analysis

As previously shown, the part of the jet with the greatest increase in activity due to cross-flow is the shear region. The narrow band (50 Hz) frequency spectra for the static pressure fluctuations in this shear region are shown in Fig. 13, for the different wind tunnel conditions. The pressure probe was placed at a position equivalent to the static case (Q = 0) for X/D = 2.5, Y/D = $\pm$ 0.5 and Z/D = 0. The spectrum for the static case shows a peak in the vicinity of 3200 Hz with a 5 dB drop per octave up to 8 kHz, where the spectrum begins to flatten out. Most of the energy for this case is in the frequency region of 1 kHz to 6 kHz. With the wind tunnel operating at a Q = 19 (V_{oo}/V_j = 0.18) there is approximately an 11 dB increase in the peak pressure which is near 2500 Hz. Beyond this peak the fall off is much faster with most of the energy lying between 1 and 4 kHz. From 15 kHz to 20 kHz there is essentially no difference between this case and the static case. As the velocity ratio is increased to 0.28 there is very little difference in the magnitude of the peak pressure, but this preak is shifted to a slightly higher frequency, approximately 3 kHz. The fall off is slightly slower than for the case Q = 19 up to 12 kHz where the two curves merge. A similar analysis was done for the pressure probe positioned in the mixing region (in the vicinity of the end of the potential cone) of the jet. For these positions the frequency spectra peaked out at 0.5 to 1 kHz.

The frequency analysis for far field microphone #3 is shown in Fig. 14. The far field curve for the static case shows a peak at approximately 1 kHz. This reflects (as mentioned above) the dominant frequency for the static pressure-fluctuation probe when placed near the potential cone of the jet wake, near the jet axis. This region, the mixing region of the jet, is known from previous experiments to be the major sound contributory to far field positions, at small angles to the jet axis. When cross-flow is inserted there is a sharp increase in the overall sound level measured at this position, even when the peaks due to the tunnel noise are ignored. The differences in levels, ignoring these peaks is approximately 10 dB for the entire spectrum, compared with the static case for a velocity ratio of 0.18; and slightly higher for a velocity ratio of 0.28. This gives one determination of jet noise increase due to cross-flow. Above 10 kHz there is a marked difference between the two velocity ratios; the frequency spectrum for 0.28 does not fall off as rapidly as that for 0.18. This is in part due to the background tunnel noise which is greater at high frequencies for Q = 47 that for Q = 19. An interesting aspect of these curves is that the peak frequency of the spectra for the velocities, again ignoring those peaks due to tunnel noise, have shifted to higher frequencies than for the static case. For V_{oo}/V_j equal 0.18 and 0.28 the peaks are near 2 kHz. This can be assumed to be a direct result of the increase activity which occurs in the shear region due to the cross-flow interaction with the jet wake. This region now becomes the dominant sound generating region. The spectra for the other three far-field microphone positions were also made and showed essentially identical characteristics to the graph in Fig. 14. This is partly due to the semi-reverberation environment of the wind tunnel.

This increase in frequency for the shear region as compared with that for the mixing region, is supported by other work. In that work a relatively slow jet is disturbed by high intensity sound fields produced at various frequencies. It is found that the maximum instability within the shear layer

occurred for a Strouhal number of 1.77 (see Fig. 10 of Ref. 10). If we compare this with the typical Strouhal number for the mixing region, 0.3, one obtains a ratio of approximately 6-1 for the critical frequencies for these two regions, agreeing qualitatively with our observations of the actual static pressure fluctuations. Because of the increased importance of the shear layer in cross-flow sound-radiation, this has the effect of increasing the frequency of the spectrum maximum for the radiated sound under cross-flow conditions. This frequency shift can be seen in Fig. 15. There for a flow ratio of 0.18 one deduces that the spectral maximum has shifted to higher values, near 2 kHz, as compared with the somewhat lower frequency maximum for no cross-flow. Incidentally some of the difficulties experienced in using the overall sound pressure levels within the wind tunnel, to determine radiating characteristics of sources located there, are clear in Fig. 15. There is an obvious interference effect at the lower frequencies; these interference effects reach up to about 2 kHz unfortunately a region of particular interest for these experiments.

The background tunnel noise for the two tunnel speeds used here is shown in Figs. 15 and 16 (microphone position #3). For comparison these graphs include the spectra of the total radiated sound when the jet is operated in cross-flow. Except in the vicinity of the sharp peaks the total radiated sound is well above the tunnel background noise. The peaks at about one and two kHz in Figs. 14 - 16 are perhaps caused by some type of whistle created by the flow interaction with some artifact in the tunnel (e.g., hole, strut, etc.). The frequencies of these peaks are proportional to the velocity of the wind tunnel. Incidentally the tunnel background noise, for the other far-field positions, was essentially the same.

3.2.3 Cross-correlation Measurements

Raw cross-correlation functions (as opposed to normalized ones) were taken between the four far field microphones and the static pressure-fluctuation probe (placed at various jet positions). The cross-correlation function times r^2 and normalized by the r.m.s. value of the static pressure fluctuations,

as described in Section 2, are plotted against velocity ratios in Figs. 17 through 20 for the six pressure probe positions recorded. The dB values are referenced to an arbitrary number and are used to give relative values. It should also be understood that the curves are derived but from three points. The error flags on these curves are calculated from the noise found on the cross-correlation functions. Since a finite averaging time is employed in the calculation of the cross-correlation functions, there exists a noise fluctuation riding on the function itself which gives the uncertainty in the true value of the cross-correlation function. The lower the cross-correlation, the higher is the uncertainty. From the graphs of the cross-correlation functions, the amplitude of the noise fluctuations was measured and used to calculate the magnitude of the error flags.

As previously mentioned, in order to make a valid comparison for the three velocity ratios employed it was necessary that the pressure probe be position-located with respect to (and aligned parallel to) the centerline of the jet wake. The probe positions chosen for the wind tunnel operating at a particular Q are equivalent to the positions stated in these plots for the static case.

Information concerning the effect of cross-flow upon the dominant noise-source regions can be obtained from Figs. 17 - 20. Additionally, we can deduce some information from these figures concerning the overall sound pressure levels. It is recalled that the data presented in these figures are obtained from cross correlation measurements; thus the far field intensities indicated there are relative values and the sounds being registered arise from the single eddy at the static pressure probe position. The typical eddy located within the shear region (X/D = 2.5 and 0:5 D off axis) radiates considerably more sound as the tunnel flow speed is increased from zero to the maximum value used here (V_{oo}/V_j = 0.28). The intensity of the sound radiated from that region (within the shear flow) increases by 10 to 20 dB for the range of V_{oo}, as seen from Figs. 17 and 18. On the other hand, the corresponding eddy located within the mixing region, at the distance X/D = 5.5, shows substantially no

change in radiating characteristics as the cross-flow speed is increased. Thus, for cross-flow we conclude that the shear region becomes a much more important radiating region (compared with the mixing zone) than is the case for the same jet without such flow. In order to determine the overall sound radiated by the jet within cross-flow, using correlations, it is necessary to add up the contributions of all such radiating regions for the whole jet. We expect the overall effect to be some average between no effect, which occurs for the mixing region, and possibly 10 - 20 dB, the increase caused by cross-flow for the shear layer. An overall increase of approximately 10 dB is consistent with these findings and bears out the conclusion from the levels measured within the wind tunnel itself.

When the pressure probe is moved out of the plane of the jet centerline and of the far field microphones, Fig. 20, the sound radiated from that eddy position shows essentially no change for far field positions #1, #2, and #3, for different velocity ratios. Far field position #4 does show an increase of approximately 10 dB when going from the static case of Q = 19. Increasing the velocity ratio results in no definite trend for this position.

The results of these cross-correlation measurements shows that the increase in activity of the shear region is mainly responsible for the additional sound generated when a jet is subjected to a cross-flow and that the sound increases by up to 10 dB due to this cross-flow.

4. CONCLUSIONS AND RECOMMENDATIONS

The primary purpose of this work was to determine the effect on sound levels when a jet is immersed in a cross-flow. A secondary purpose has been to develop, in a preliminary way, a measurement process employing correlation techniques, which could be used in a reverberant wind tunnel environment.

Cross-flow on a jet has been found here to cause a 10 dB increase in the radiated sound. This increase was essentially the same for the two tunnel speeds. This is determined in several different ways. First, this was done using the overall sound levels as measured within the wind tunnel. The sound levels measured within the wind tunnel include reverberant effects i.e., reflections from the tunnel walls. One expects the reflections to be proportional to the strength of the radiating source so that relative values can be significant for these tests, provided that the jet noise exceeds tunnel background. Other workers[9] have found a 6 dB increase in levels as a result of cross-flow, in the 40'x80' wind tunnel. The relative comparisons probably were approximately valid there also. The smaller change observed in that work may have been due to the high background noise in the large tunnel. In our tests the tunnel background was well below the jet noise, except for the pure tones already discussed.

We saw from the cross-correlation measurements made on the jet in cross-flow, that for sound radiated from the shear region there was an increase of from 10 to 20 dB; the sound radiated from the mixing region was not much affected by the cross flow according to these measurements. Furthermore the increase in sound was not much dependent upon which of the two tunnel speeds was employed, again indicating that the noise increase in cross flow may not be critically dependent upon the cross flow speed.

There is another way in which we got some information concerning the effect of cross-flow on jet noise characteristics. We saw that the static

pressure fluctuations increased by from 7 to 10 dB in the shear layer for the jet with cross flow (and that this increase did not depend upon which of the two tunnel speeds was being used). Using the basic pressure source theory this leads to a predicted increase of 14 to 20 dB for jet with cross-flow flow. (There was little increase of static pressure fluctuation within the mixing regions of the jet.) These increases are consistent with those discussed above.

To obtain information about the effect of cross-flow on jet noise directivity, we compare microphones 1 and 4 under cross-flow conditions. Using cross-correlation measurements it was seen that there was little directivity effect for the (dominant) shear region sources; for the mixing regions we saw an effect of up to 5 dB, comparable to the effect found using jets in an anechoic room.

It was found that the peak of the spectrum of the sound radiated by the jet with cross-flow shifted upward by as much as a factor of 5. This is attributed to the dominant effect of the higher-frequency shear layer source regions as a result of cross-flow influences.

Finally, a comment concerning the correlation measurement technique: The difficulties experienced in making sound level measurements within reverberant wind tunnels are sufficiently displayed within this report. The correlation measurement process has the advantage that it can eliminate background noses and unwanted reflection noise. However, the smaller the signal to noise (referring to the directly radiated sound as the signal and all other sounds whether reflections or otherwise as noise) then the greater the averaging time needed in order to obtain a valid correlation.

Many of our measurements could have been improved (if the scope of the work had permitted) by such increased averaging times. It is recommended that this method be pursued in the future; the averaging-time increases

required are not large: Frequently a factor of three would suffice. There is every indication that the method can be fruitful in deducing anechoic-type results from the data one actually obtains in wind tunnels.

REFERENCES

1. W. C. Meecham, and G. W. Ford, "Acoustic Radiation from Isotropic Turbulence", J. Acoust. Soc. Am. 30, 1958, pps. 318-322.

2. H.S. Ribner, "The Generation of Sound by Turbulent Jets", Advances in Appl. Mech., 8 , 103 (1964).

3. W. C. Meecham, "A Fluid Mechanics View of Aerodynamic Sound Theory", Loughborough University of Technology, Loughborough, Leiceistershire, England 1970.

4. T. D. Scharton and W. C. Meecham, "Preliminary Experimental Investigation of the Simple Source Theory of Jet Noise", J. Acoust. Soc. Am. 51, pps. 383-386, (1972)

5. T. D. Scharton and P.H. White, "The Simple Pressure Source Model of Jet Noise", To be published in the J. Acoust. Soc. Am.

6. P. M. Hurdle, W. C. Meecham, and B. Hodder, "Pressure Cross-correlations Measured on a Jet Engine", Paper to be published in the J. Acoust. Soc. Am., November 1974.

7. T. E. Siddon, Proceedings of INTER-NOISE 1972 Conference, Oct. 4-6, 1972, Washington, D.C., pps. 452-457.

8. R. J. Margason, "The Path of a Jet Directed at Large Angles to a Subsonic Free Stream", Langley Research Center, NASA TND-4919.

9. D.L. Stimpert and R.G. Fogg, "Effect of Cross Flow Velocity on The Generation of Lift Fan Jet Noise in VTOL Aircraft," NASA CR 114571, Feb. 1973.

10. D. Bechert and E. Pfizenmaier, "Optical Compensation Measurements on The Unsteady Exit Condition at a Nozzle Discharge Edge," to be published J. Fluid Mechanics.

11. P. M. Hurdle, "Pressure Cross-Correlations in the Investigation of Aerodynamic Noise from Jets", Ph.D. Thesis, UCLA, 1973.

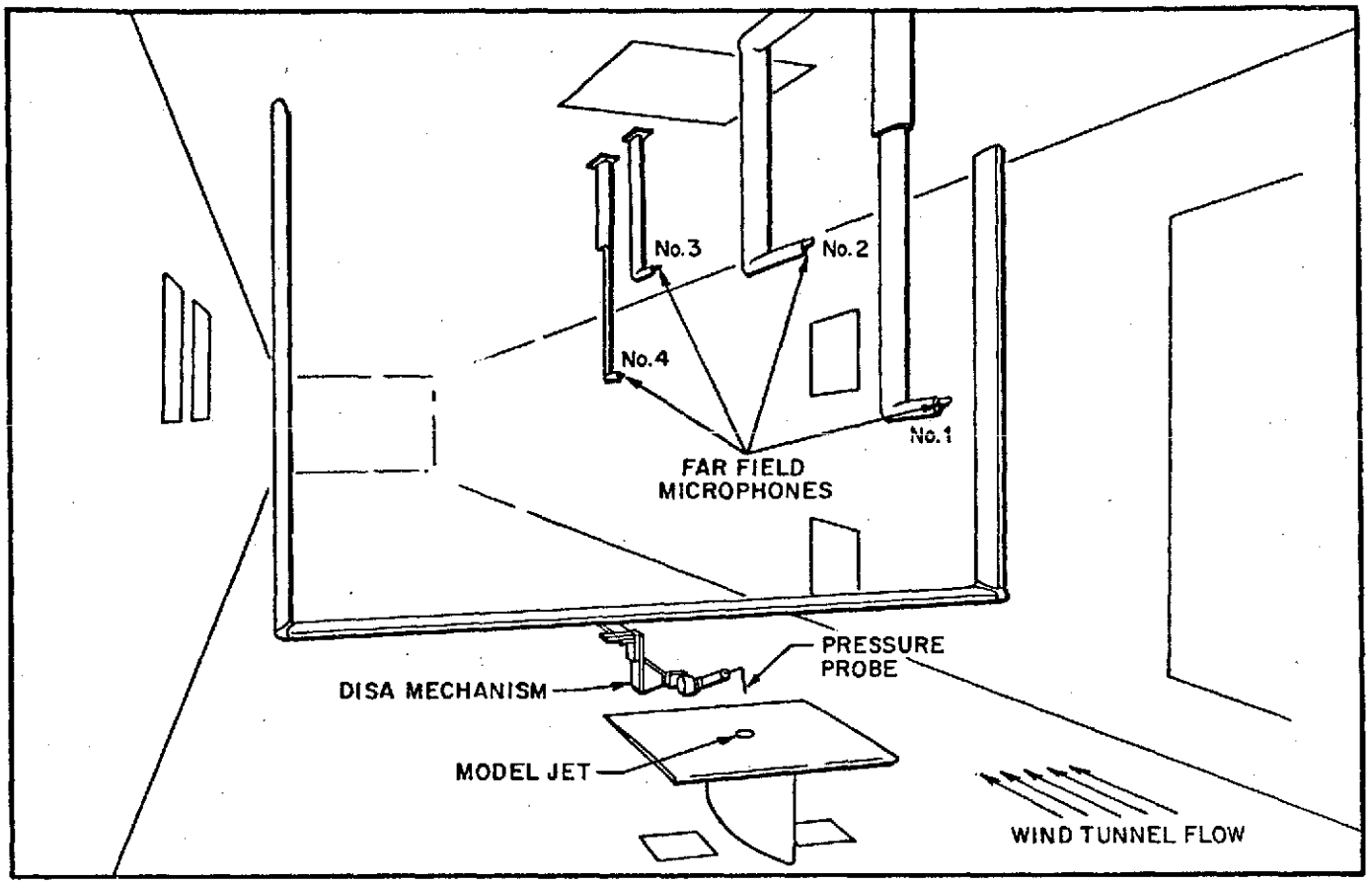

Figure 1a . Perpendicular Jet Experiment.

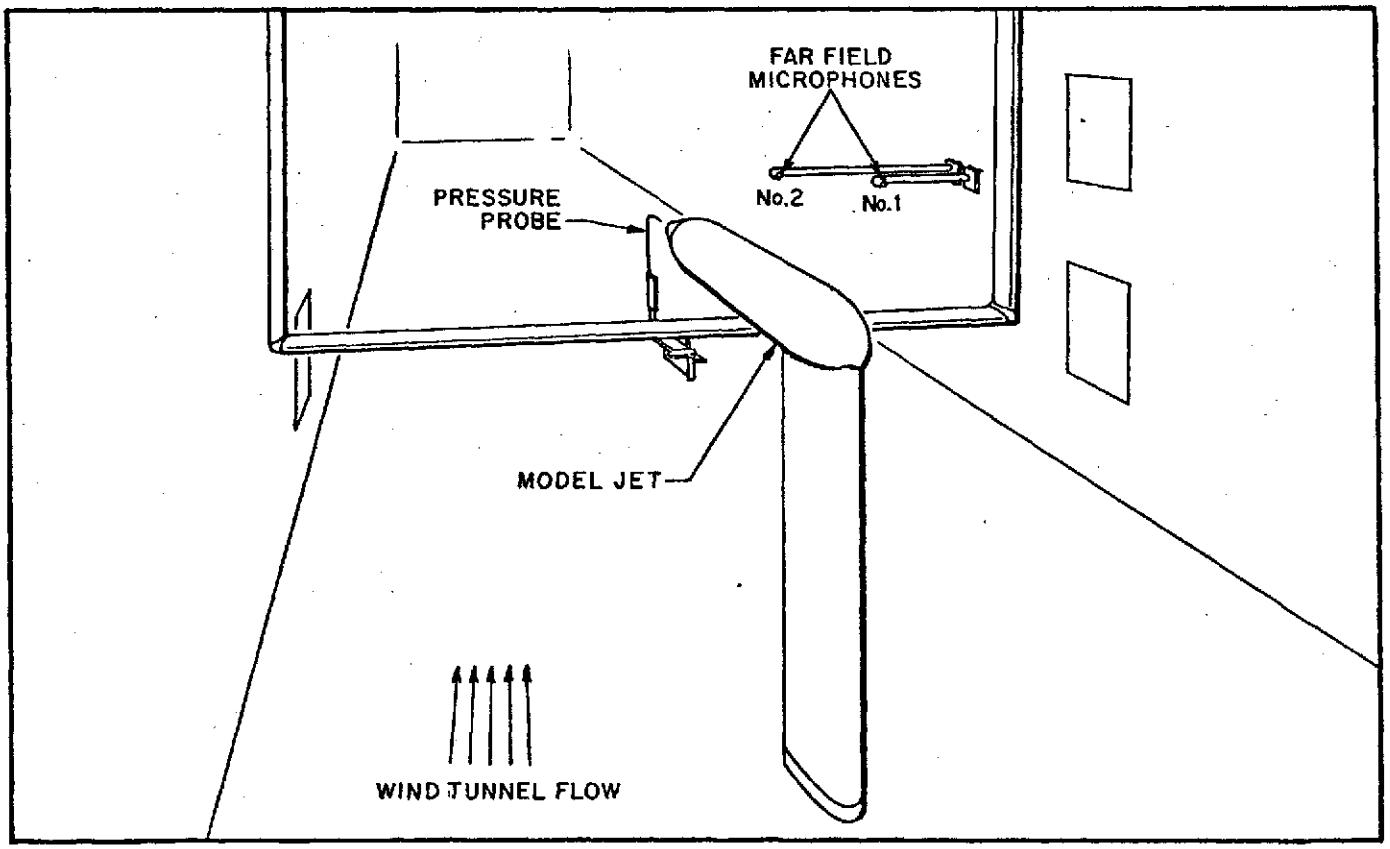

Figure 1b . Parallel Jet Experiment.

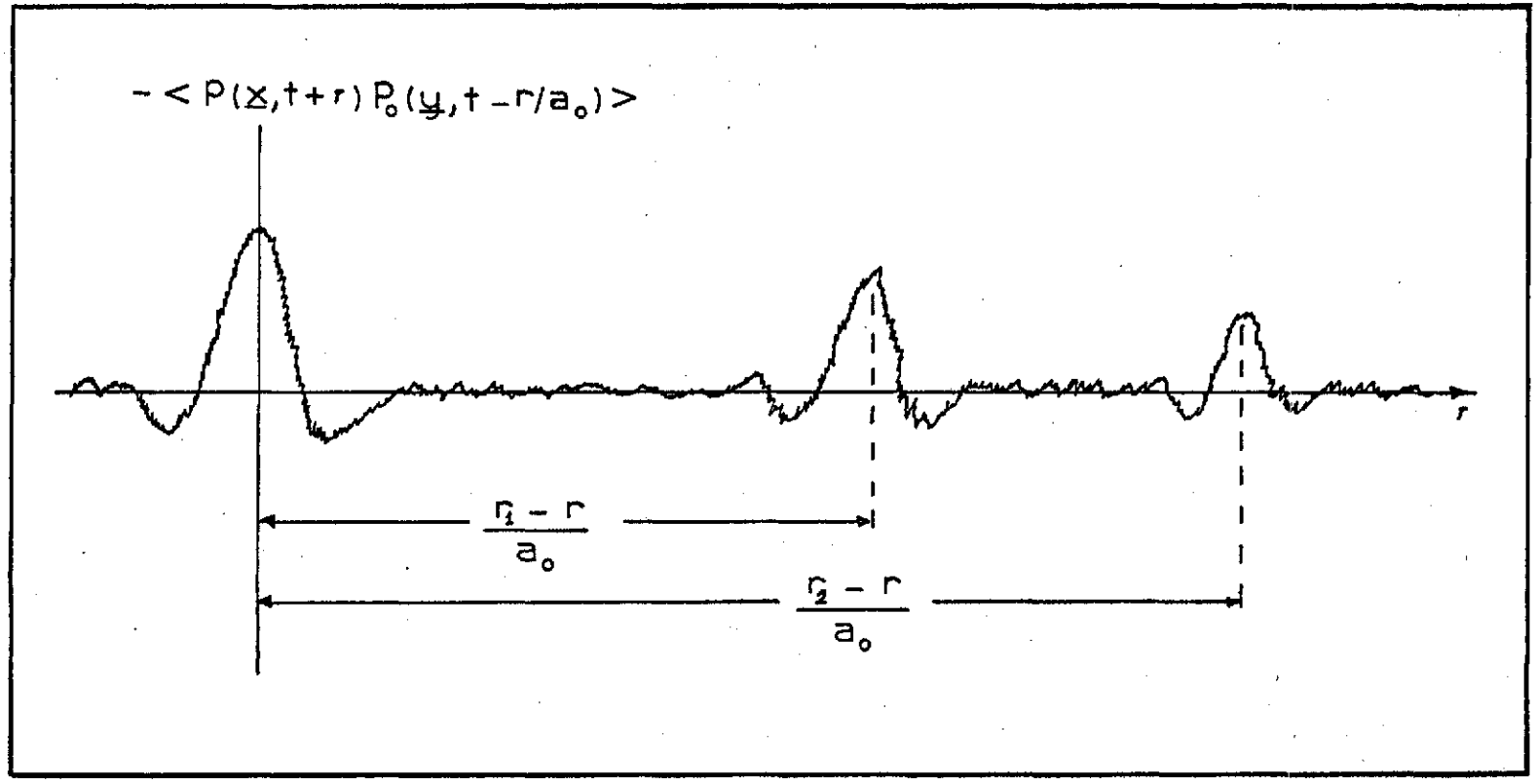

Figure 2 . Reverberant Cross-correlation.

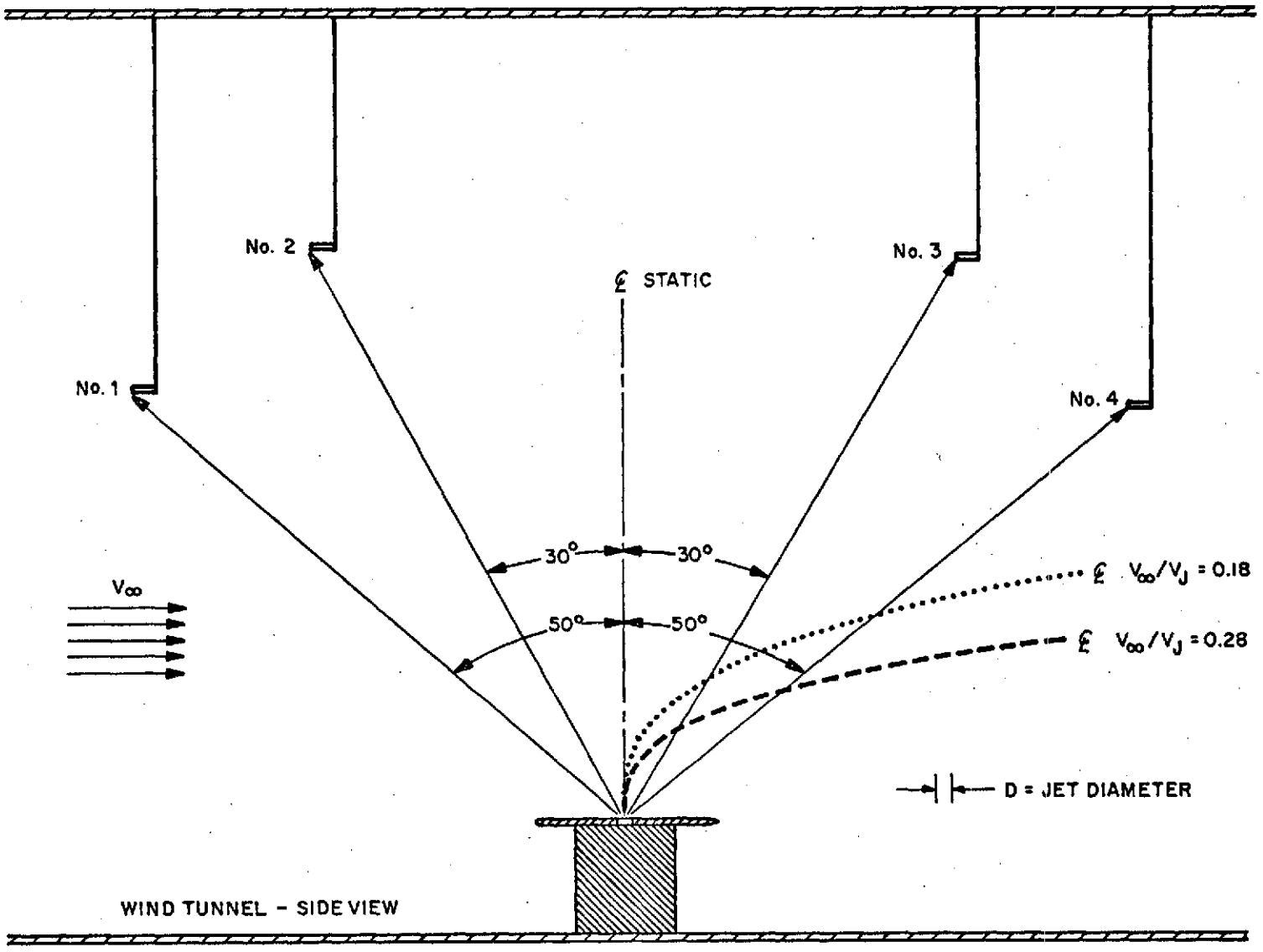

Figure 3 . Test Geometry for Perpendicular Jet.

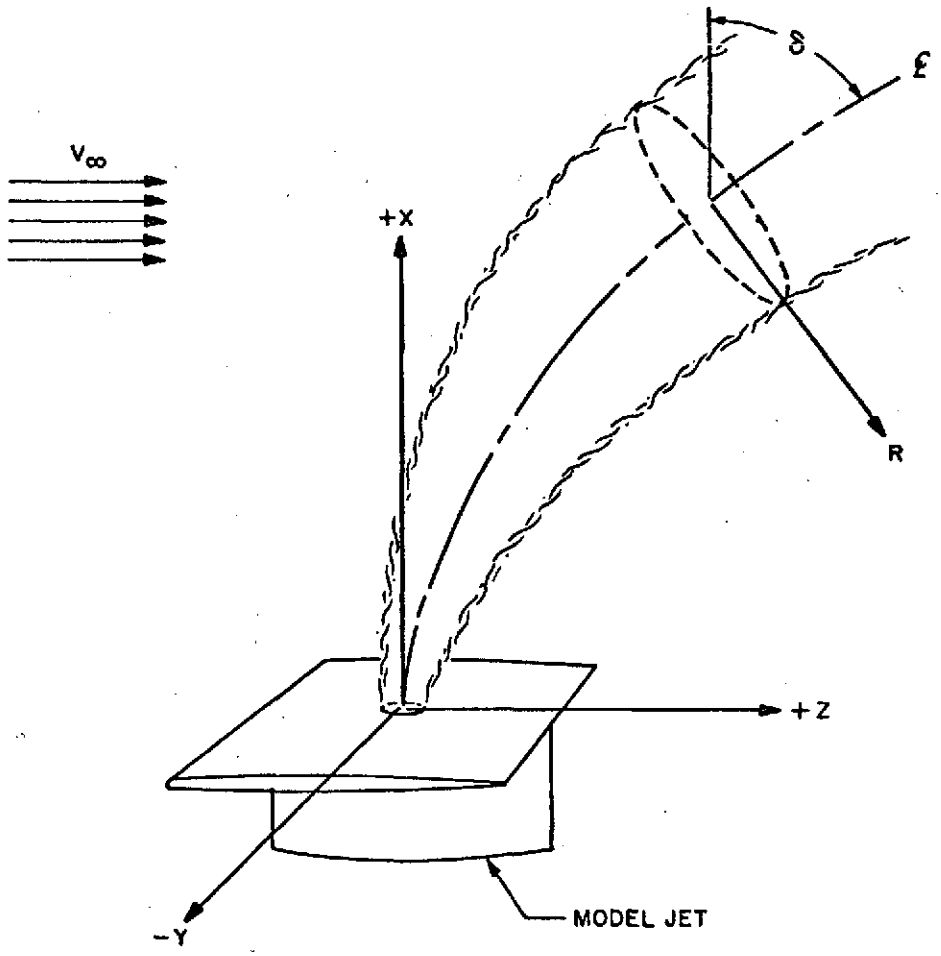

Figure 4 . Pressure Probe Coordinate System for Perpendicular Jet.

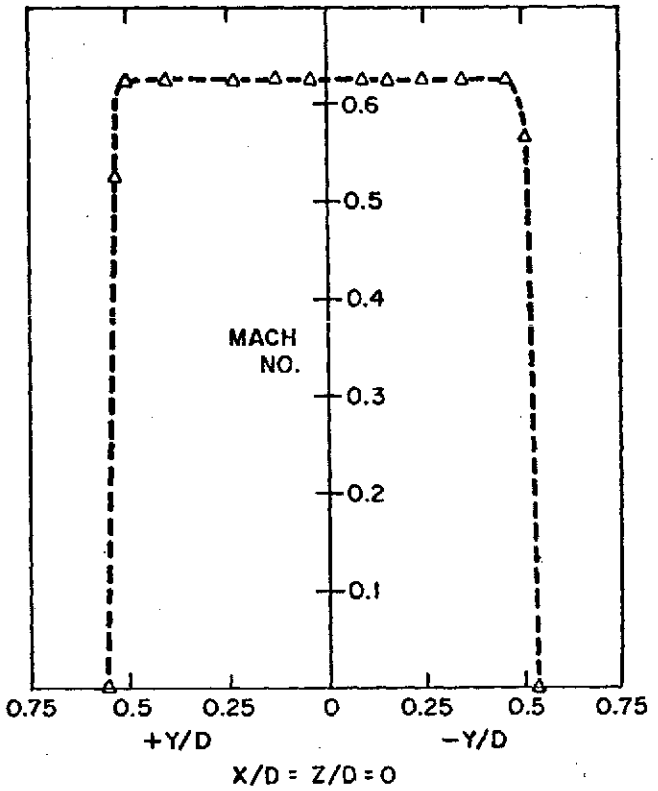

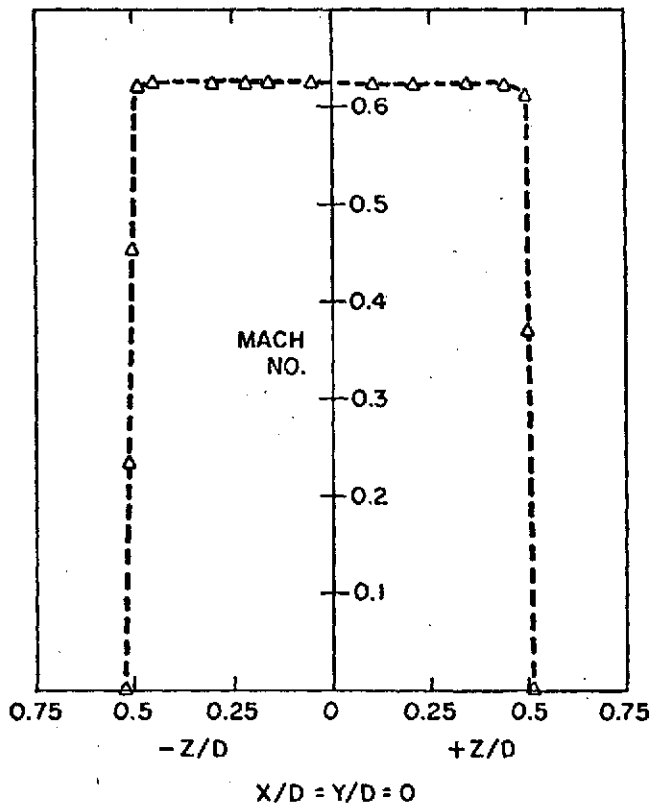

Figure 5 . Velocity Profiles for Perpendicular Jet.

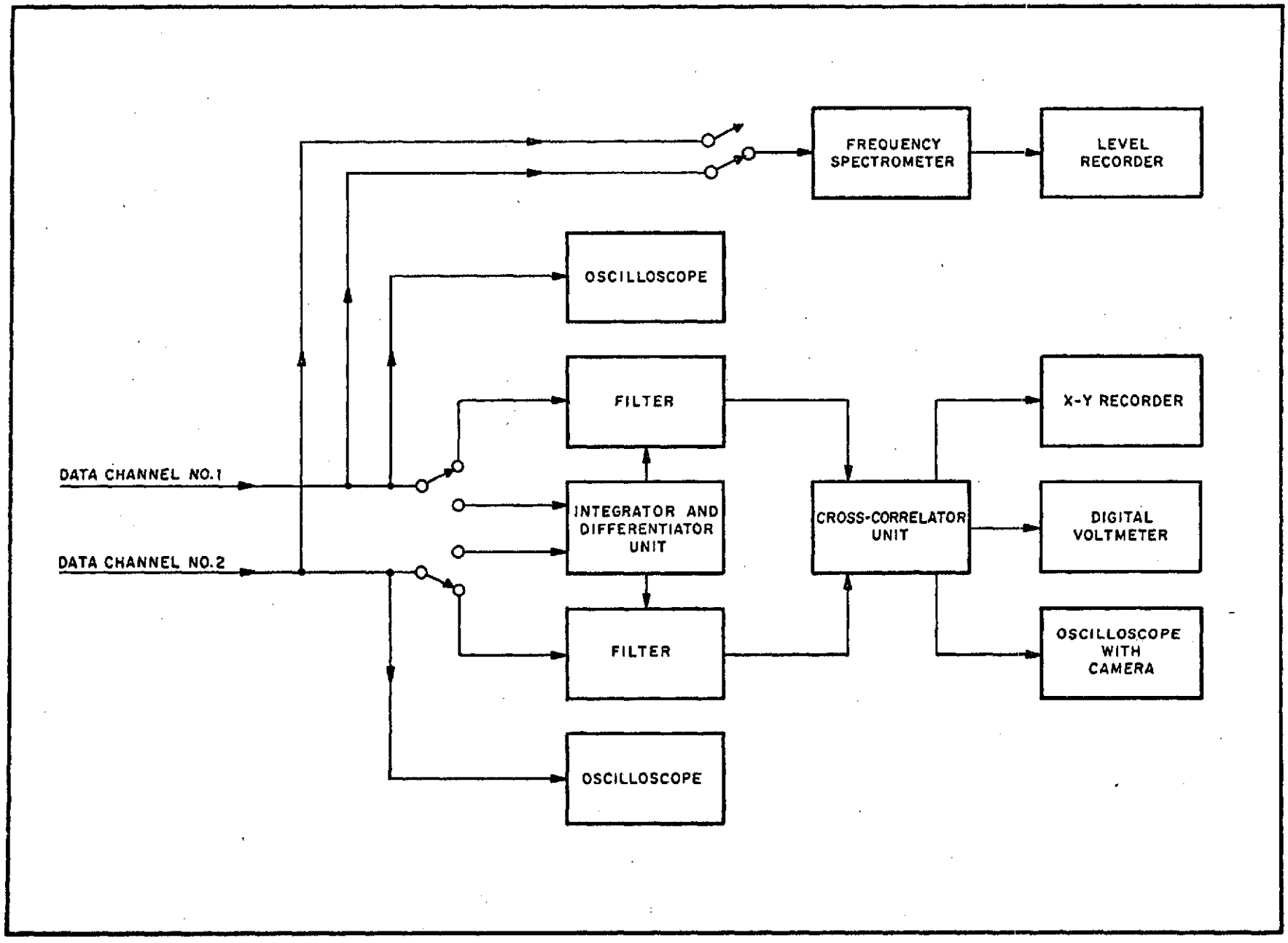

Figure 6. Block Diagram of Equipment for Data Analysis.

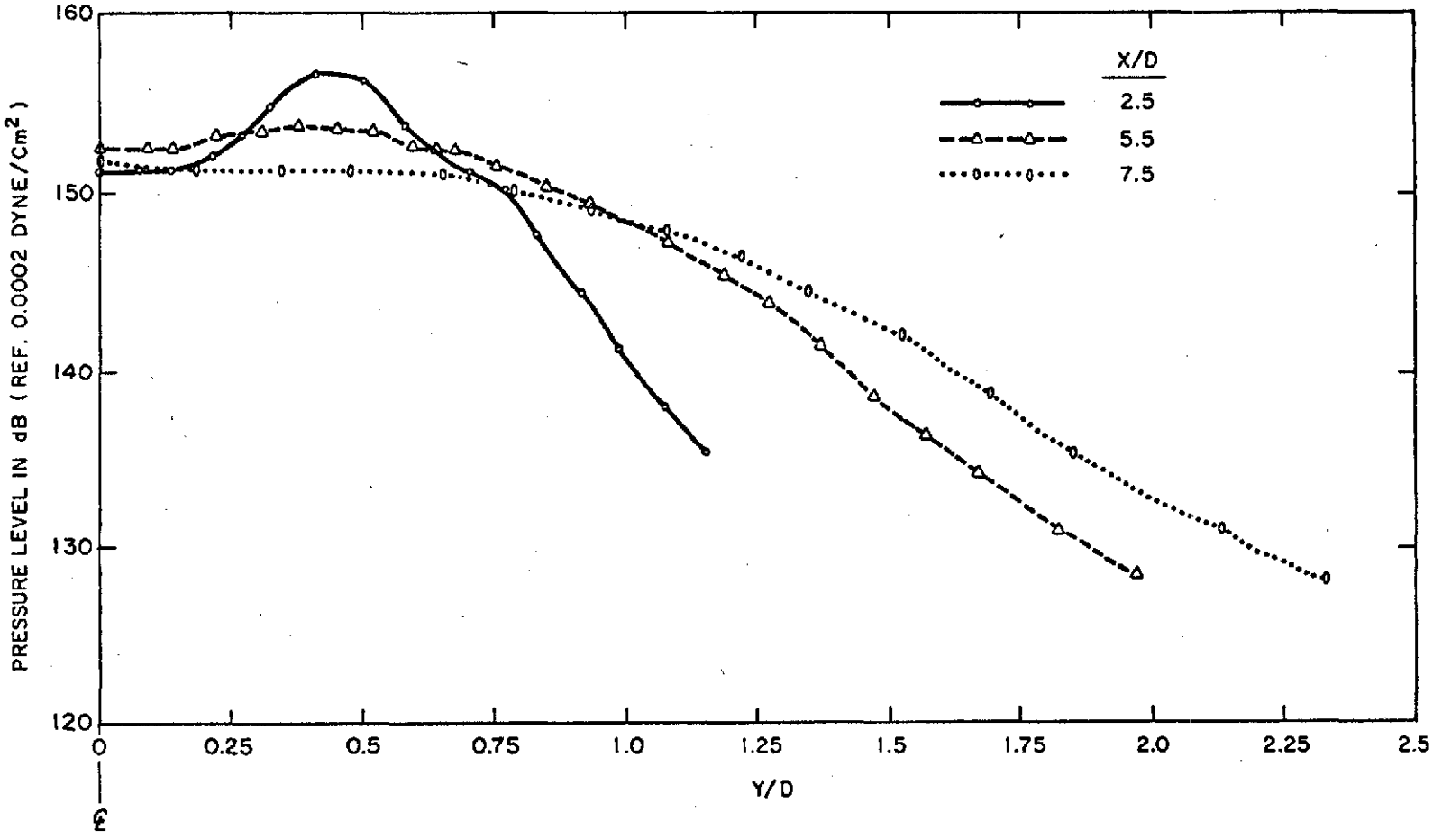

Figure 7 . Static Pressure Fluctuations Profiles for Perpendicular Jet with Tunnel Q Equals Zero.

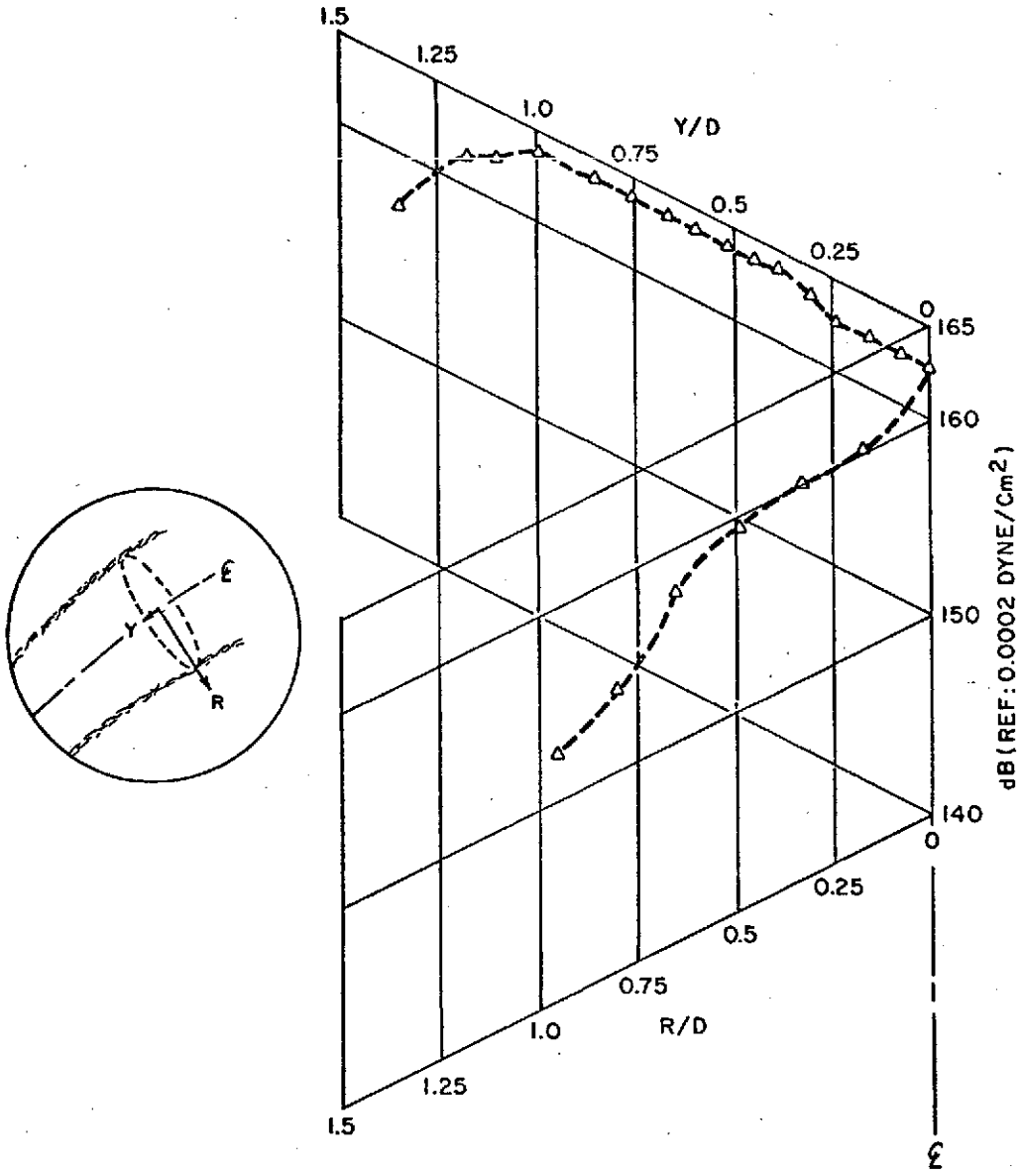

Figure 8 . Static Pressure Fluctuations Profile for Perpendicular Jet with $V_\infty / V_J = 0.18$.
(℄ probe position: X/D = +2.5, Y/D = 0.0, Z/D = +0.18, $\delta = 9^o$)

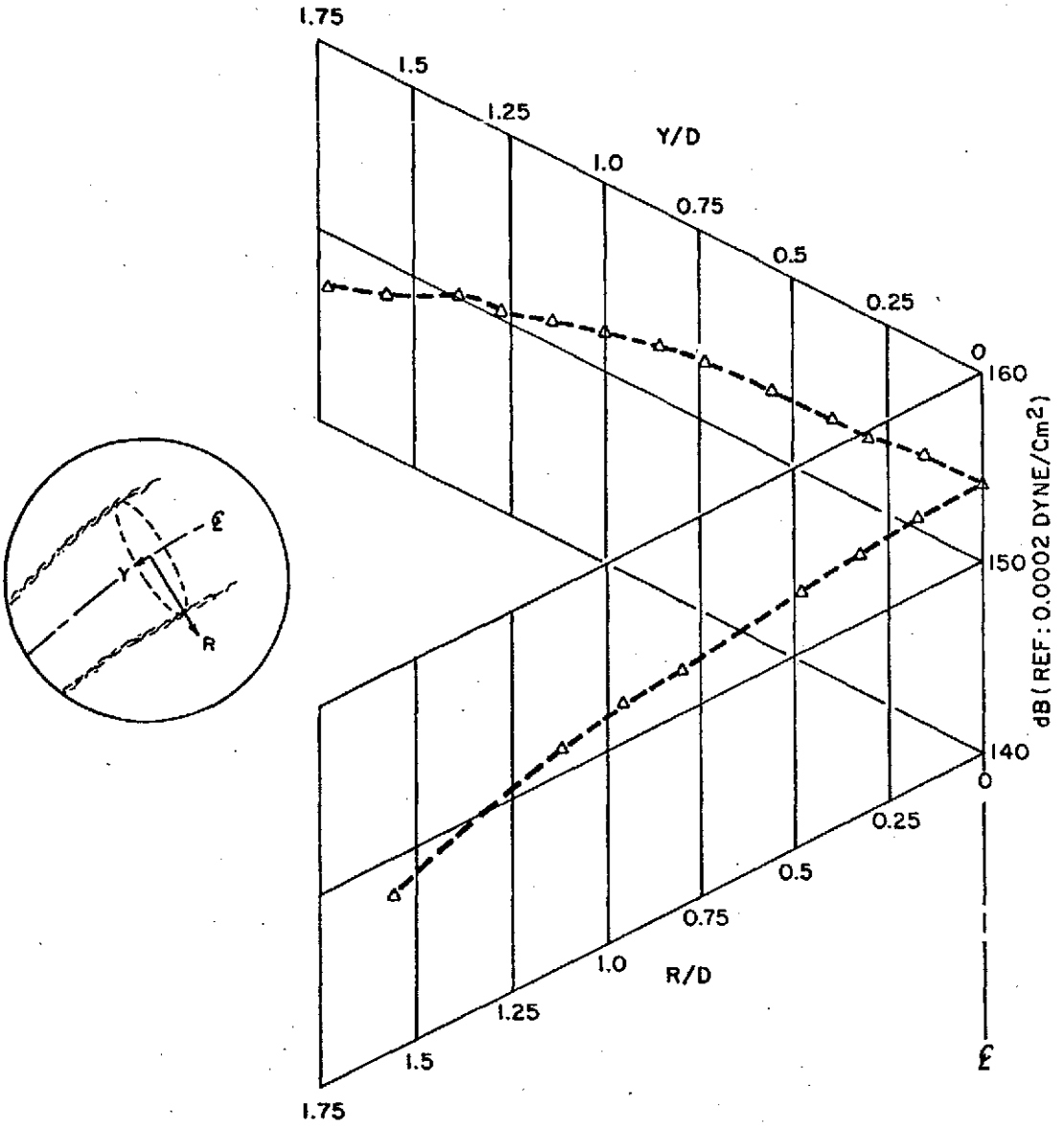

Figure 9 . Static Pressure Fluctuations Profile for Perpendicular Jet with $V_\infty / V_J = 0.18$.
(℄ probe position: X/D = +5.3, Y/D = 0.0, Z/D = +1.2, $\delta = 34^\circ$)

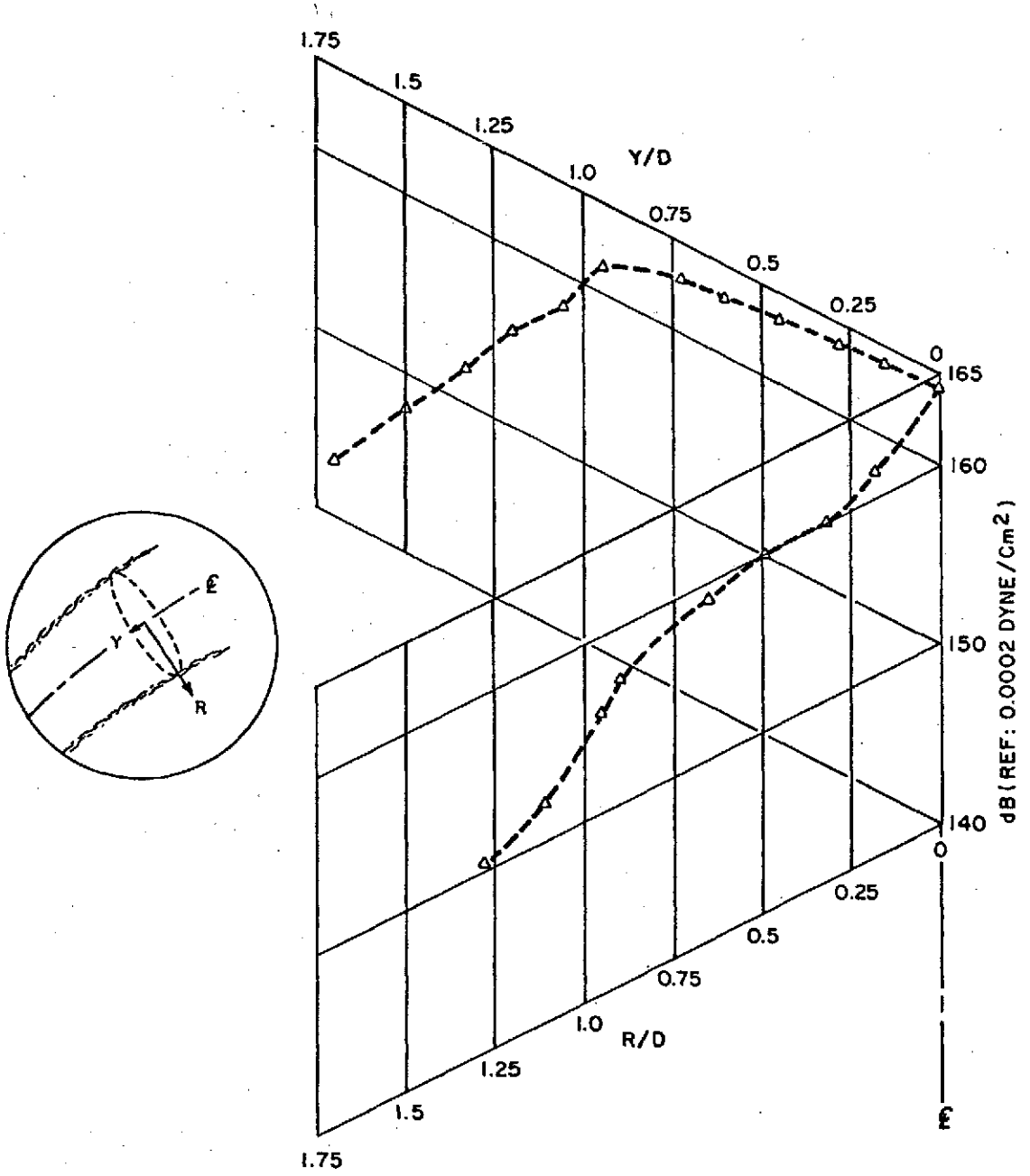

Figure 10 . Static Pressure Fluctuations Profile for Perpendicular Jet with $V_\infty / V_J = 0.28$.
(℄ probe position: X/D = +2.3, Y/D = 0.0, Z/D = +0.22, $\delta = 16^\circ$)

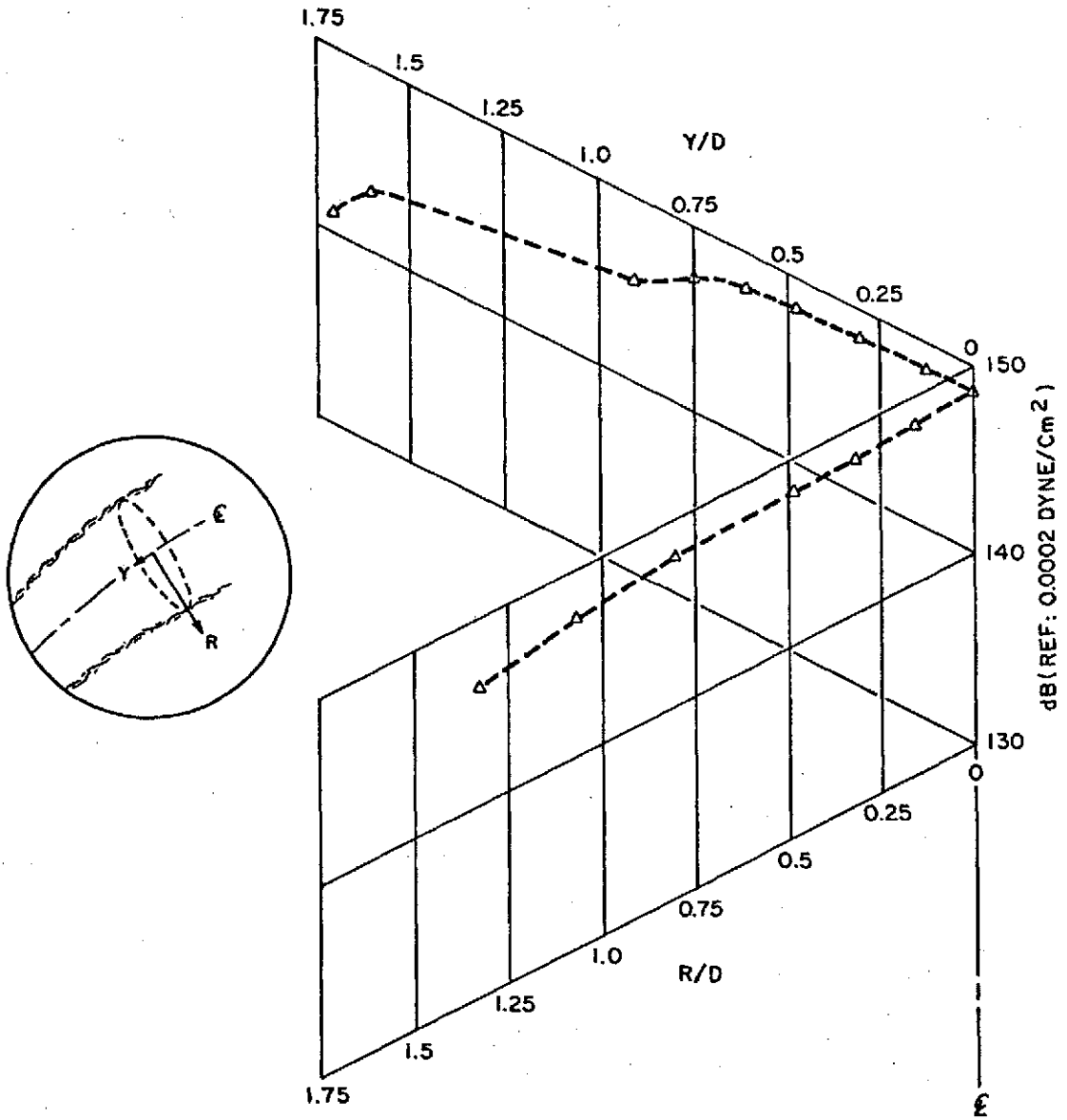

Figure 11 . Static Pressure Fluctuations Profile for Perpendicular Jet with $V_\infty / V_J = 0.28$.
(℄ probe position: X/D = +4.66, Y/D = 0.0, Z/D = +3.41, $\delta = 53^\circ$)

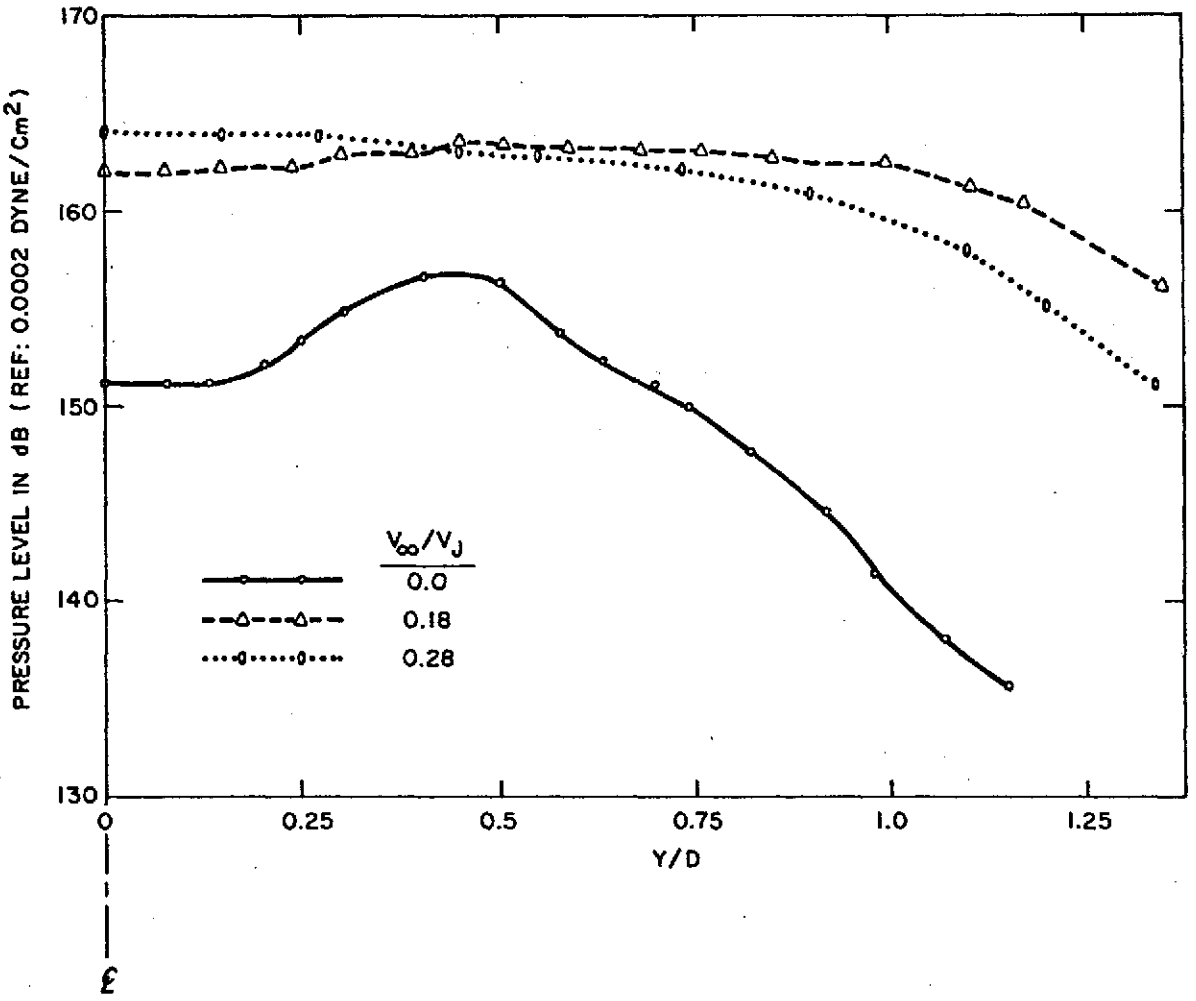

Figure 12 . Static Pressure Fluctuations Profiles for Perpendicular Jet with Different Wind Tunnel Conditions.
(Probe position equivalent to static case of X/D = +2.5 & Z/D = 0.0)

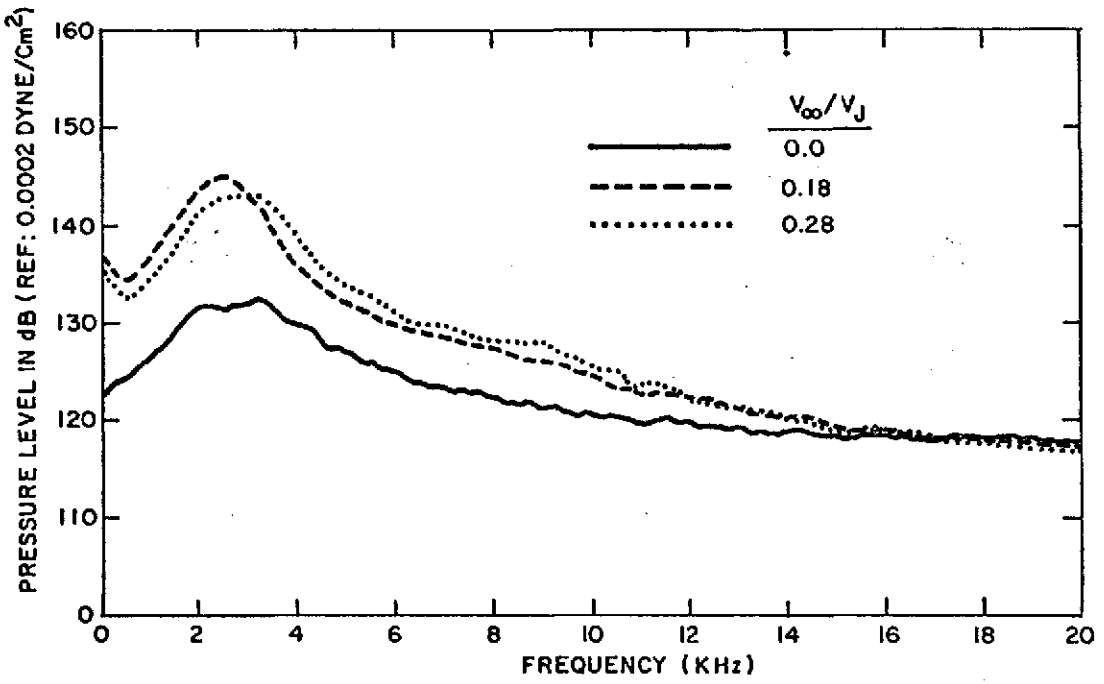

Figure 13 . Narrow Band (50 Hz.) Frequency Spectra of Static Pressure Fluctuations for Perpendicular Jet with Different Wind Tunnel Conditions. (Probe position equivalent to static case of X/D = +2.5, Y/D = ±0.5, & Z/D = 0.0)

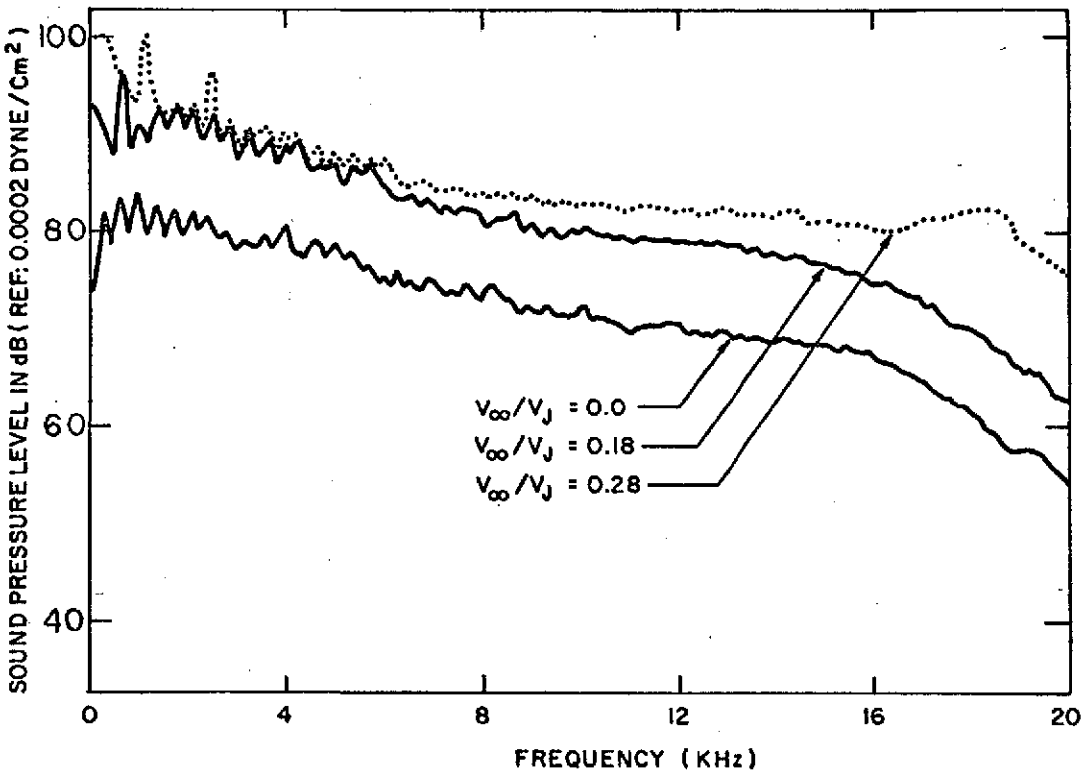

Figure 14 . Narrow Band (50 Hz.) Frequency Spectra of Far Field Radiated Sound for Perpendicular Jet with Different Wind Tunnel Conditions. (Far Field Microphone #3)

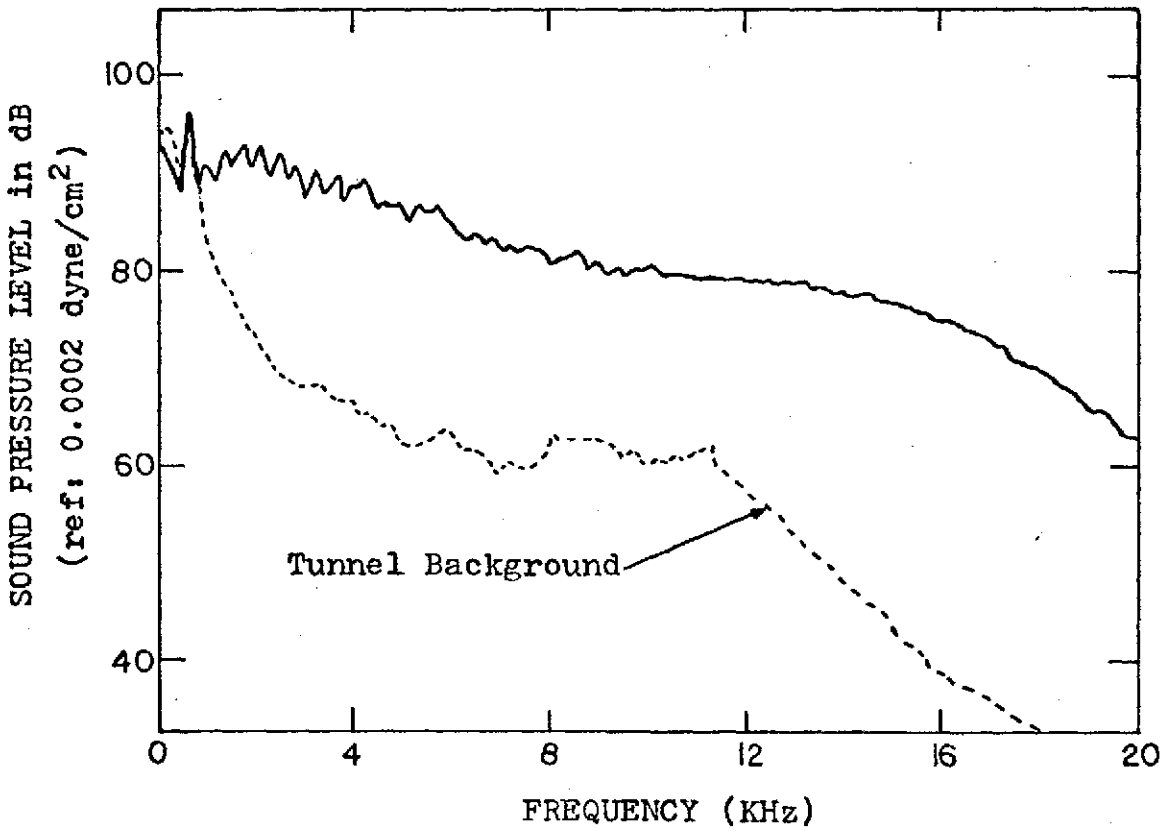

Figure 15. Narrow Band (50 Hz) Frequency Spectra of Tunnel Background Noise (V_∞ = 38.4 m/sec) and Far Field Radiated Sound for Perpendicular Jet (V_∞/V_J = 0.18). (Far Field Microphone #3)

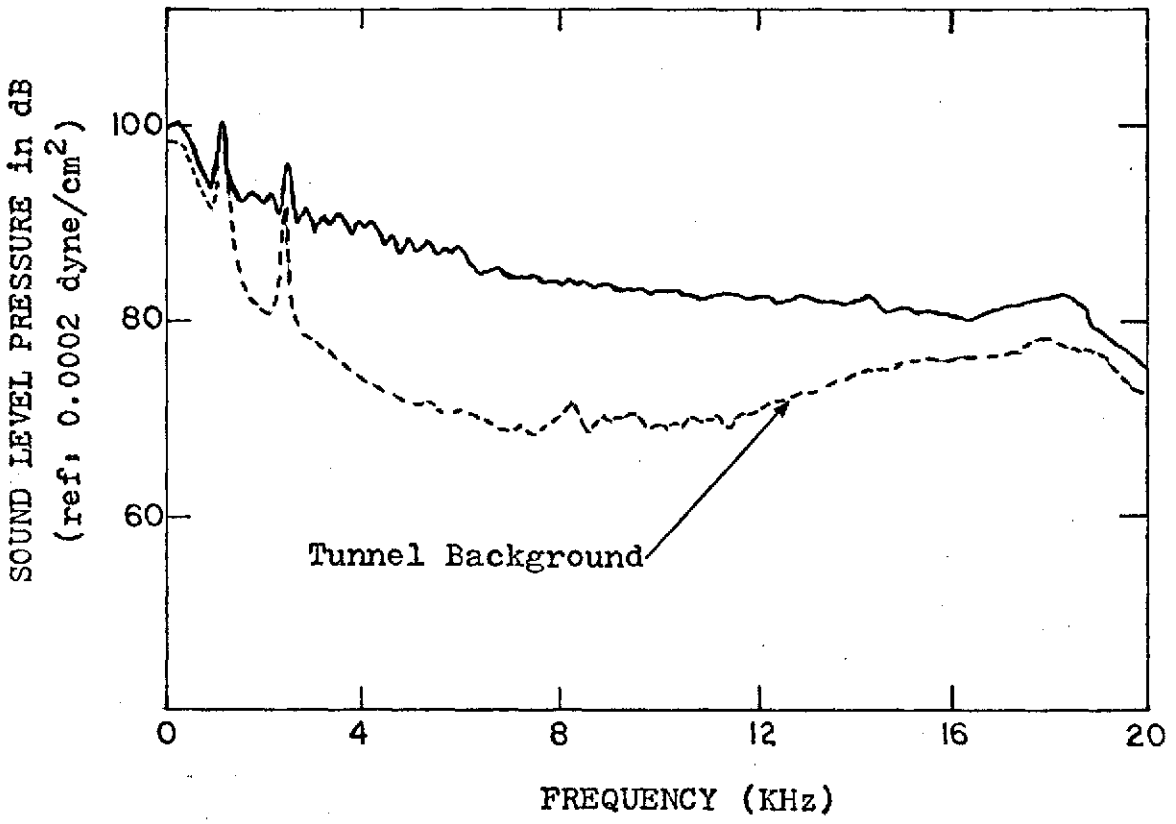

Figure 16 . Narrow Band (50 Hz) Frequency Spectra of Tunnel Background Noise (V_∞ = 60.4 m/sec) and Far Field Radiated Sound for Perpendicular Jet (V_∞/V_J = 0.28).
(Far Field Microphone #3)

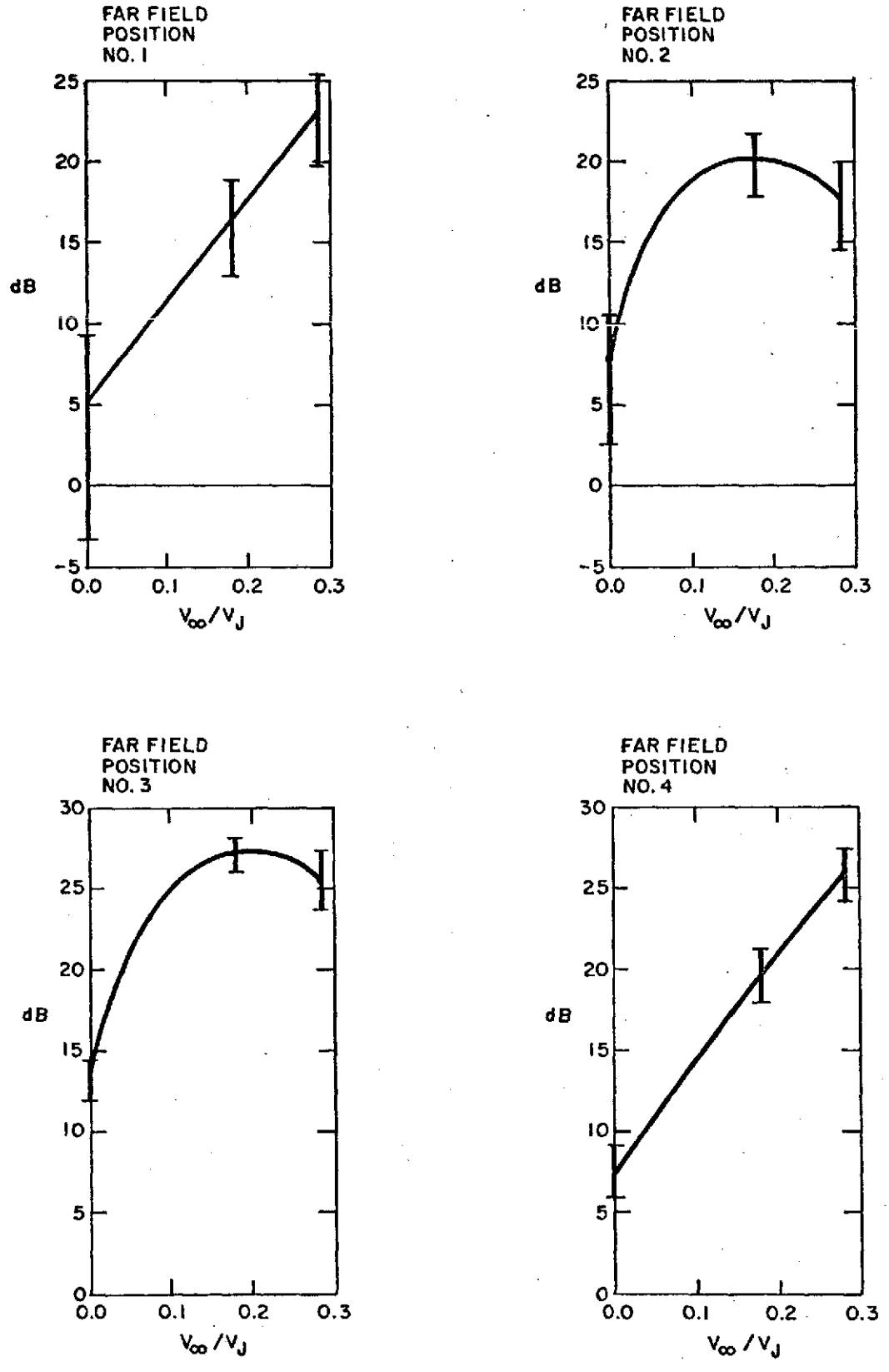

PROBE POSITIONS EQUIVALENT TO STATIC CASE: X/D = 2.5 , Y/D = 0.0 , Z/D = + 0.5

Figure 17 . Effect of Tunnel Speed Variate on the Sound Radiated from the Eddy at the Probe Position for Perpendicular Jet.

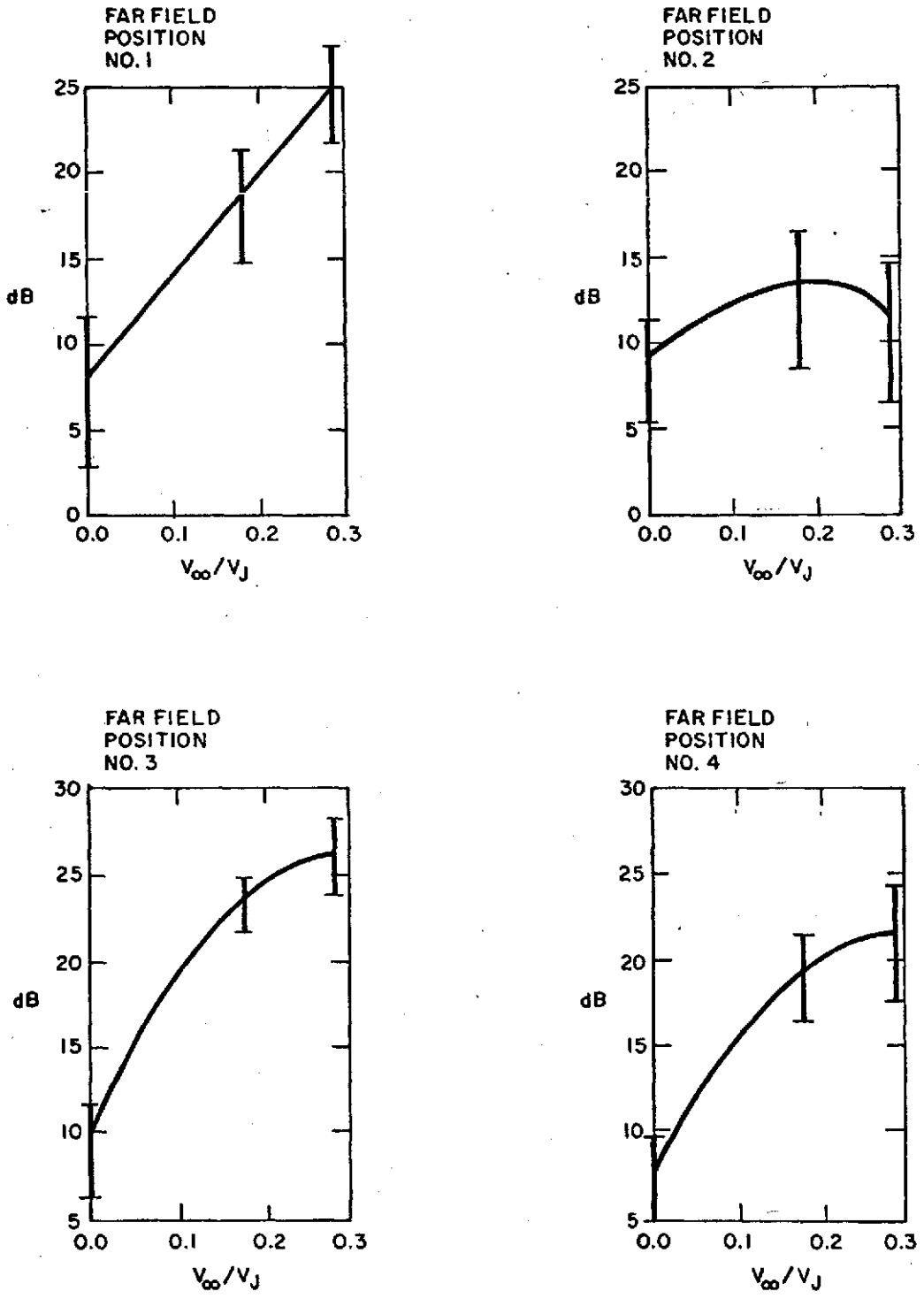

PROBE POSITIONS EQUIVALENT TO STATIC CASE : X/D = 2.5, Y/D = ±0.5, Z/D = 0.0

Figure 18 . Effect of Tunnel Speed Variate on the Sound Radiated from the Eddy at the Probe Position for Perpendicular Jet.

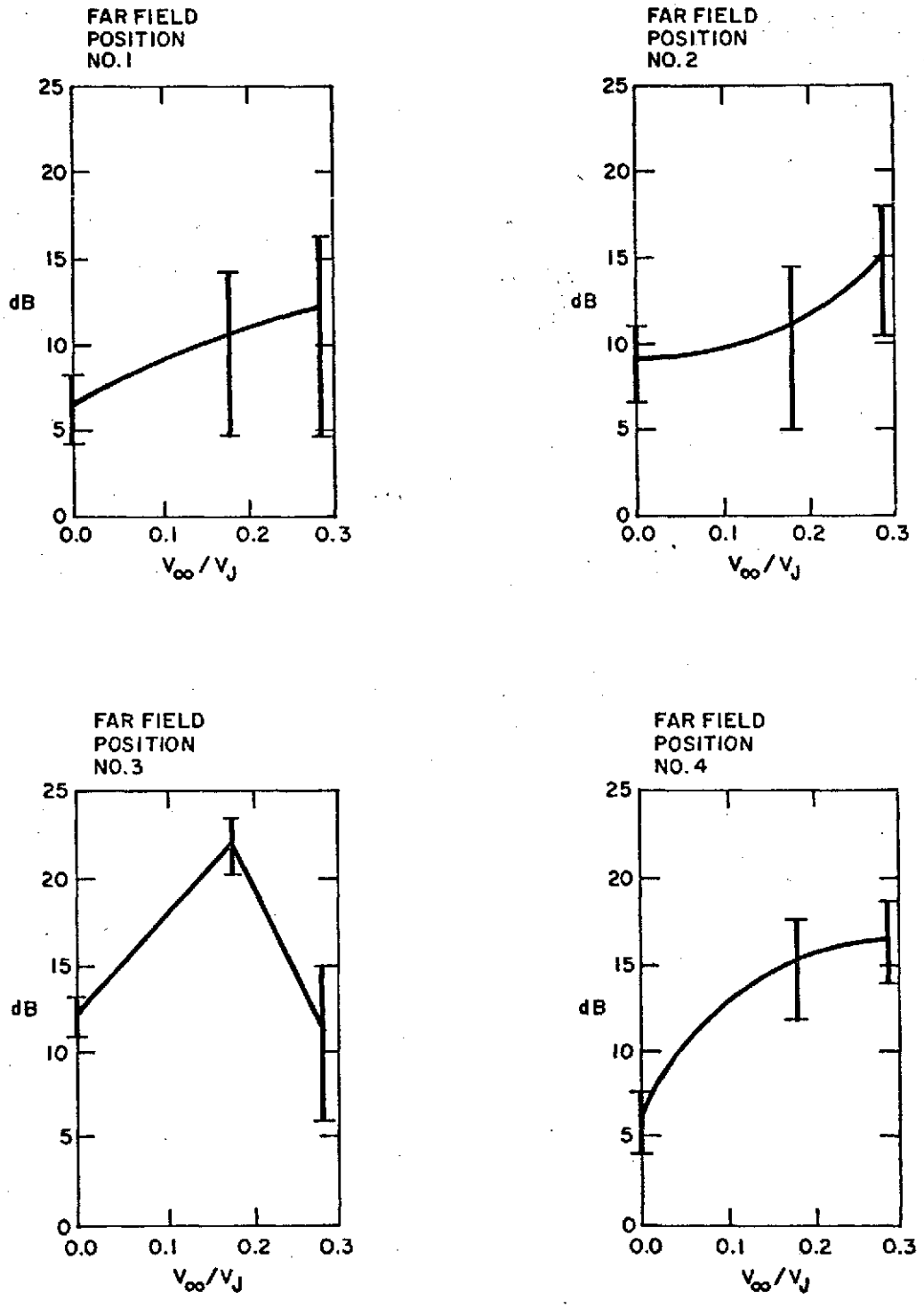

PROBE POSITIONS EQUIVALENT TO STATIC CASE : X/D = 5.5 , Y/D = 0.0 , Z/D = 0.0

Figure 19 . Effect of Tunnel Speed Variate on the Sound Radiated from the Eddy at the Probe Position for Perpendicular Jet.

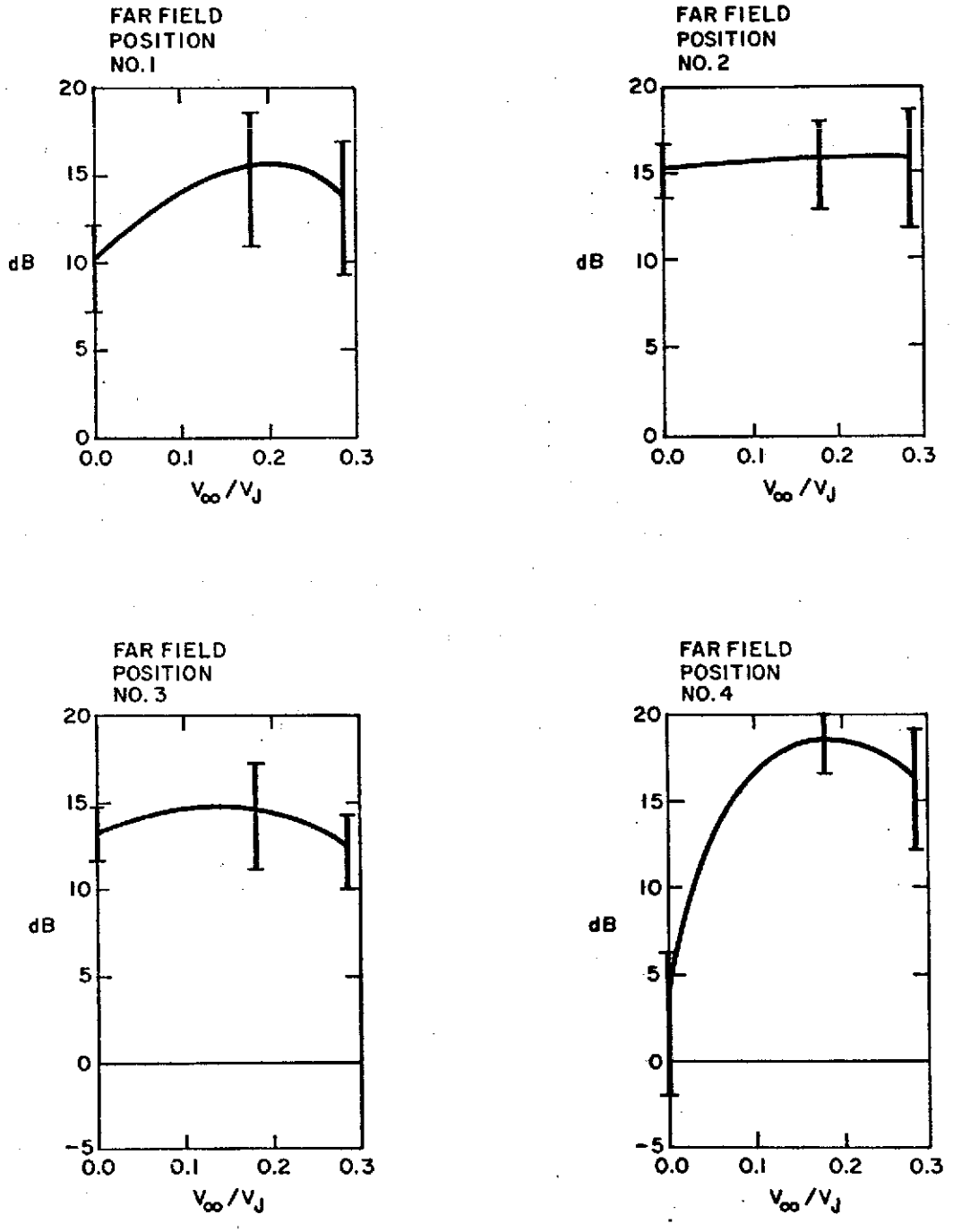

PROBE POSITIONS EQUIVALENT TO STATIC CASE: X/D = 5.5, Y/D = ±0.33, Z/D = 0.0

Figure 20 . Effect of Tunnel Speed Variate on the Sound Radiated from the Eddy at the Probe Position for Perpendicular Jet.

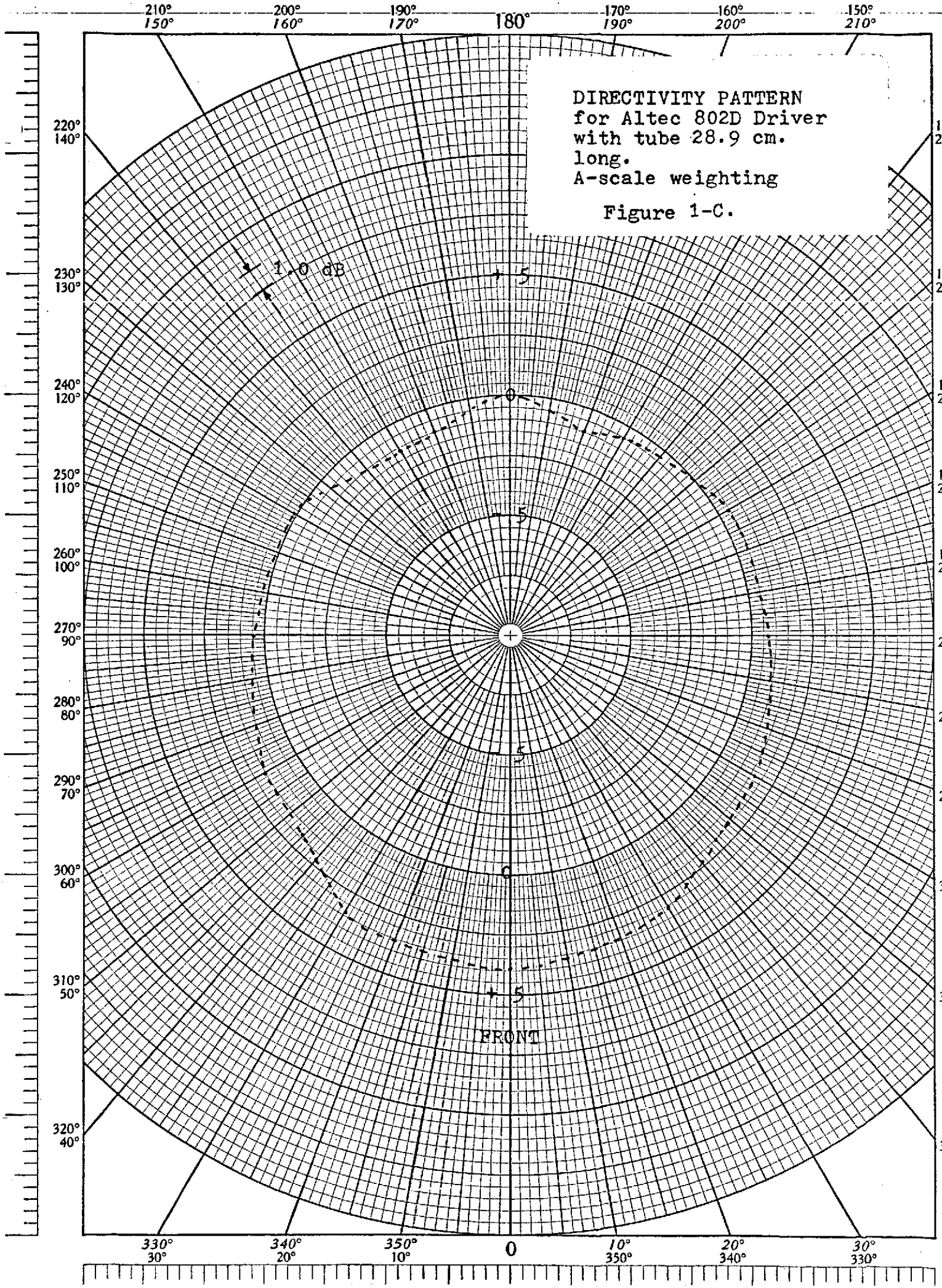
DIRECTIVITY PATTERN
for Altec 802D Driver
with tube 28.9 cm.
long.
A-scale weighting
Figure 1-C.
1.0 dB
FRONT
180°
0
210° 150°
200° 160°
190° 170°
170° 190°
160° 200°
150° 210°
220° 140°
230° 130°
240° 120°
250° 110°
260° 100°
270° 90°
280° 80°
290° 70°
300° 60°
310° 50°
320° 40°
140° 220°
130° 230°
120° 240°
110° 250°
100° 260°
90° 270°
80° 280°
70° 290°
60° 300°
50° 310°
40° 320°
330° 30°
340° 20°
350° 10°
10° 350°
20° 340°
30° 330°
5
5
5
5
0
POLAR CO-ORDINATE 359-31
KEUFFEL & ESSER CO. MADE IN U.S.A.

TABLE 1-C

Corrected Normalized Cross-correlation Values for 7'x 10' Wind Tunnel Measurements.

Probe & Mic #	Source Orientation	Uncorrected $c(x,\tau)$ Tunnel	Corrected $c(x,\tau)$ Tunnel	$c(x,\tau)$ Anechoic Chamber	Error %
1	vertical	.537	1.011	.892	+13.4
1	canted	.599	1.084	.848	+27.8
2	canted	.407	.817	.820	-0.4
4	vertical	.499	1.034	.885	+16.9
4	canted	.430	.902	.873	+3.3

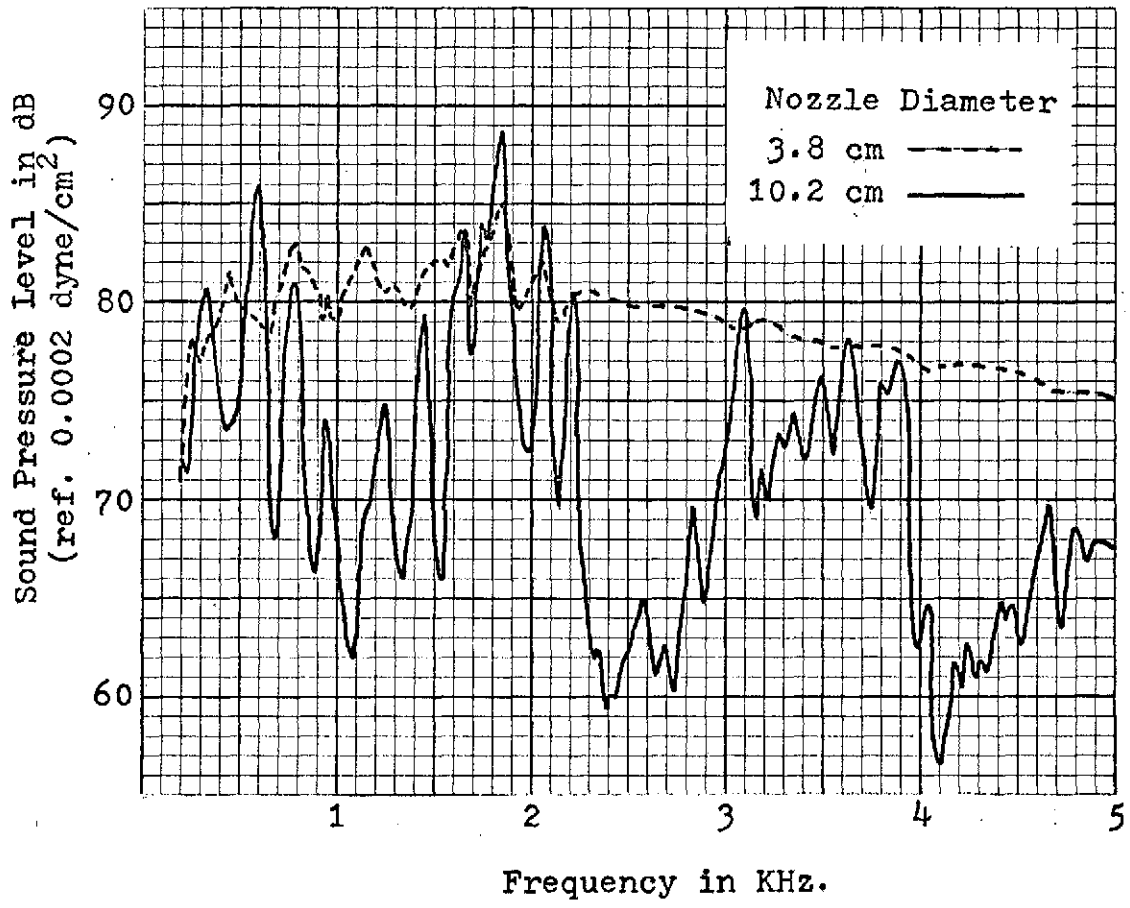

Figure 1-D. Frequency spectrum of sound pressure from model jet with different nozzle diameters.
(constant bandwidth: 50 Hz.)

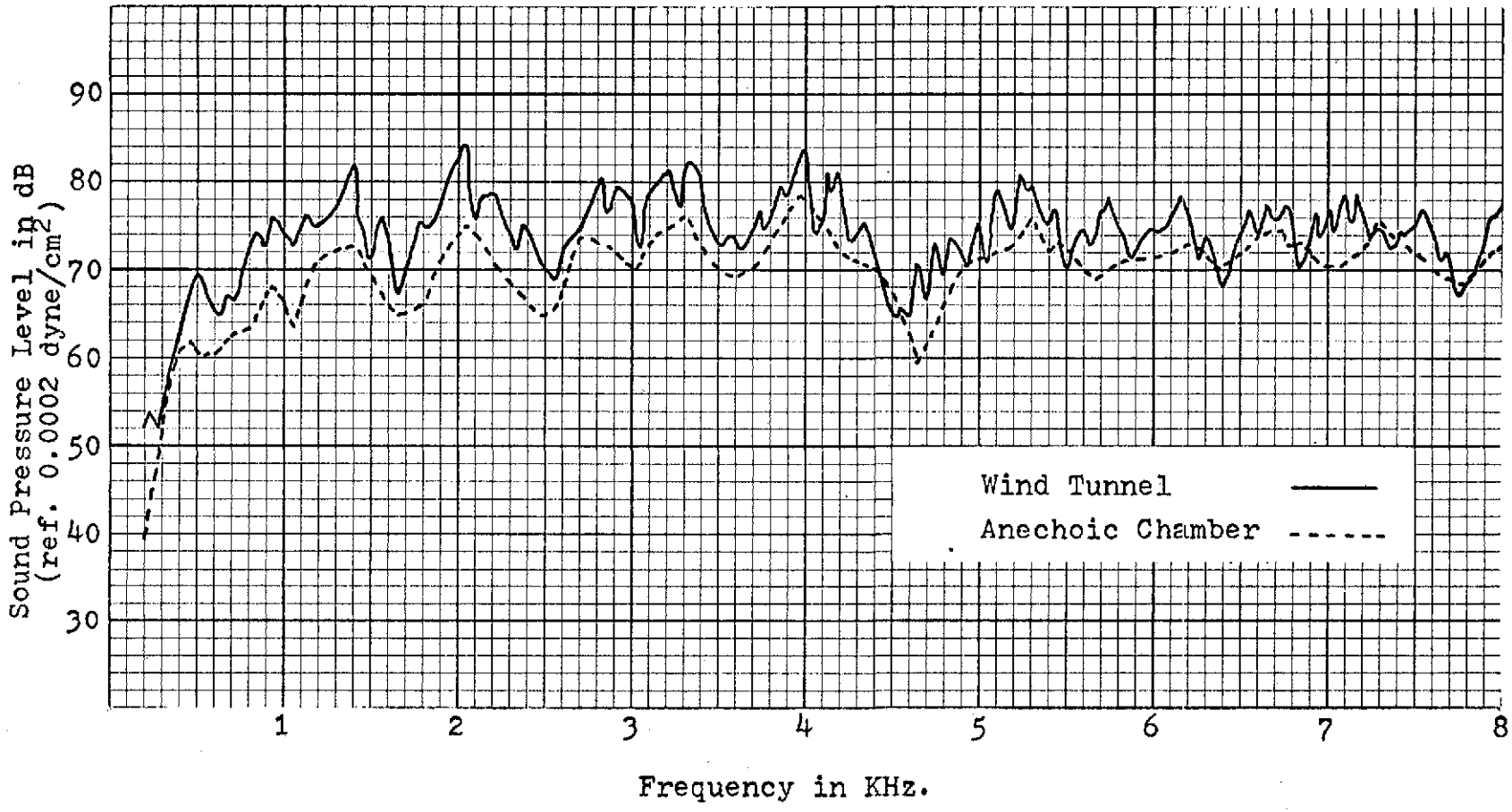

Figure 2-C. Frequency spectrum of sound pressure from simple source in anechoic chamber and 7'x10' wind tunnel. (constant bandwidth: 50 Hz.)

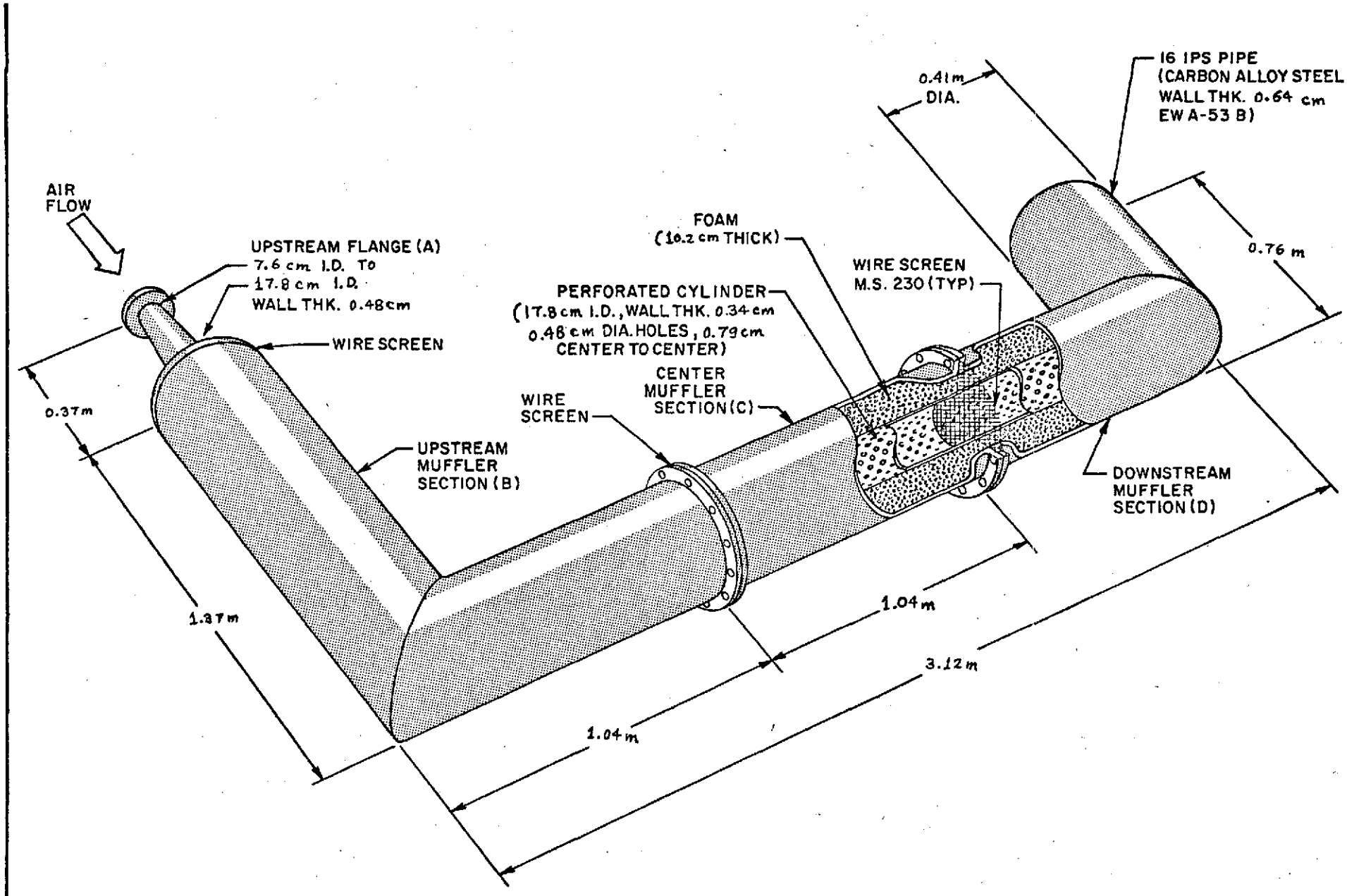

Figure 2-D. Acoustic Muffler for Model Jet in 7'x 10' Wind Tunnel.

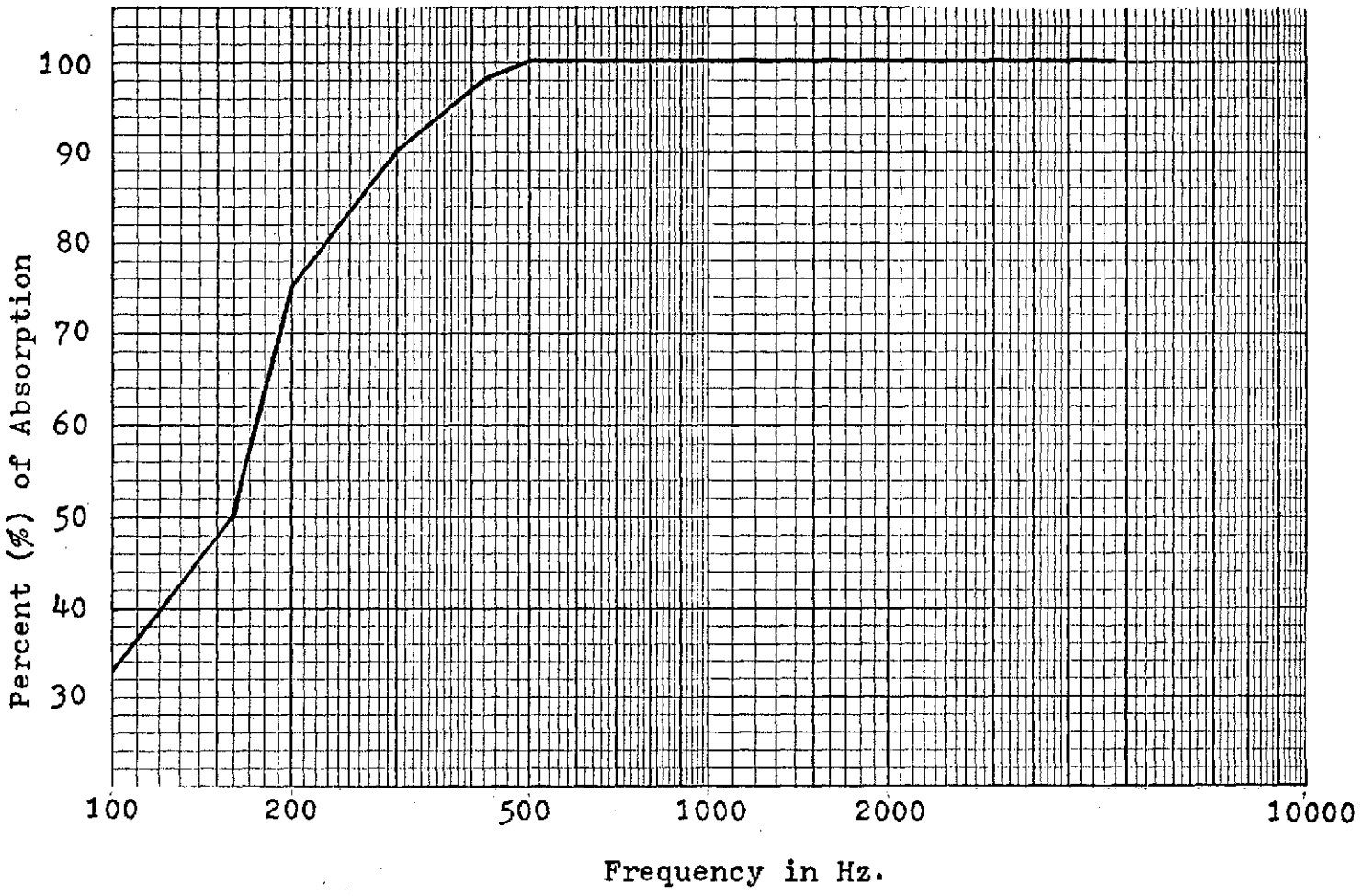

Figure 3-D. Random Absorption for 10.2 cm thick Genereal Acoustics Foam.

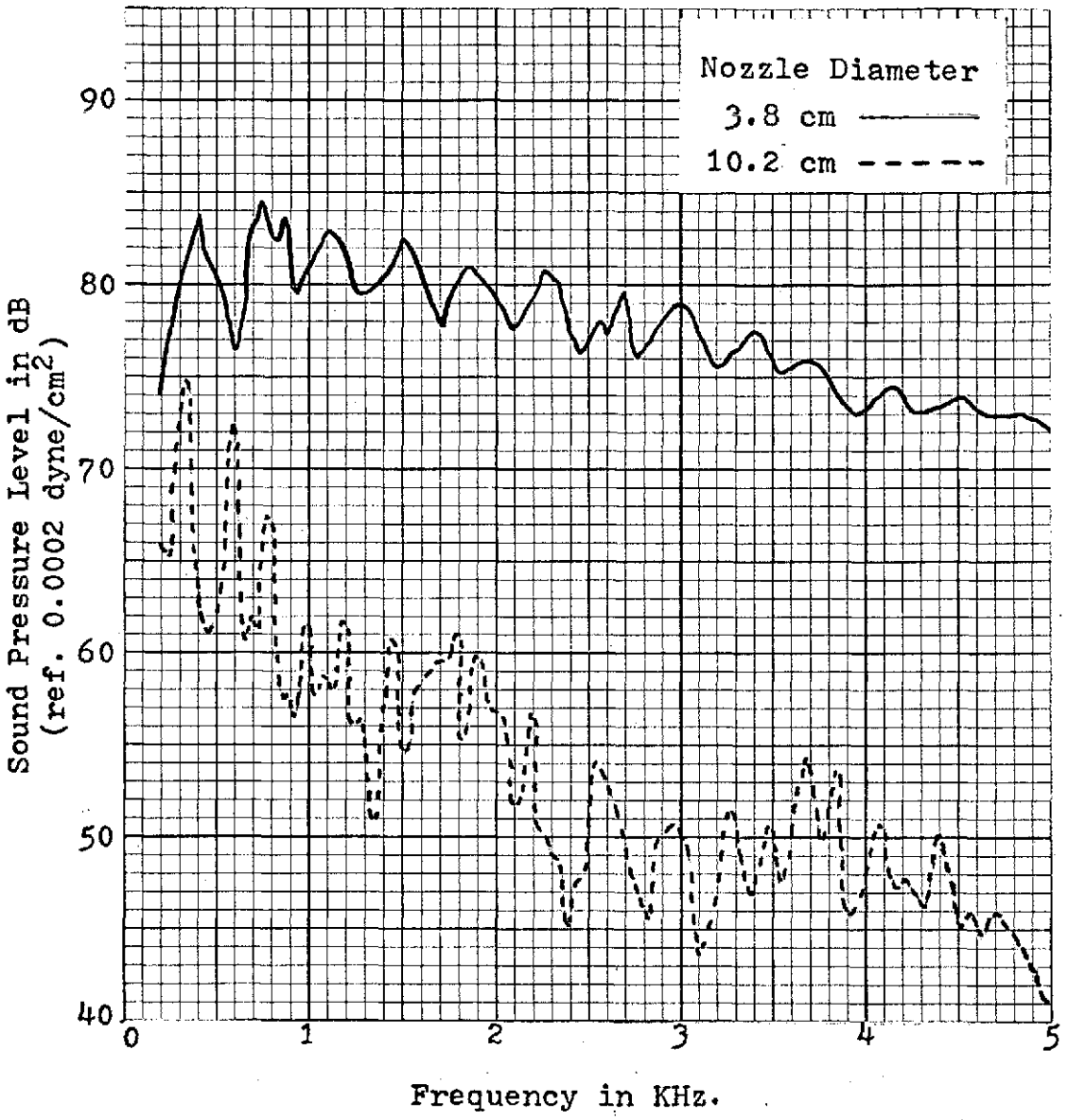

Figure 4-D. Frequency spectrum of sound pressure from model jets with different nozzle diameters. Model jets equipped with acoustic muffler. (constant bandwidth: 50 Hz.)

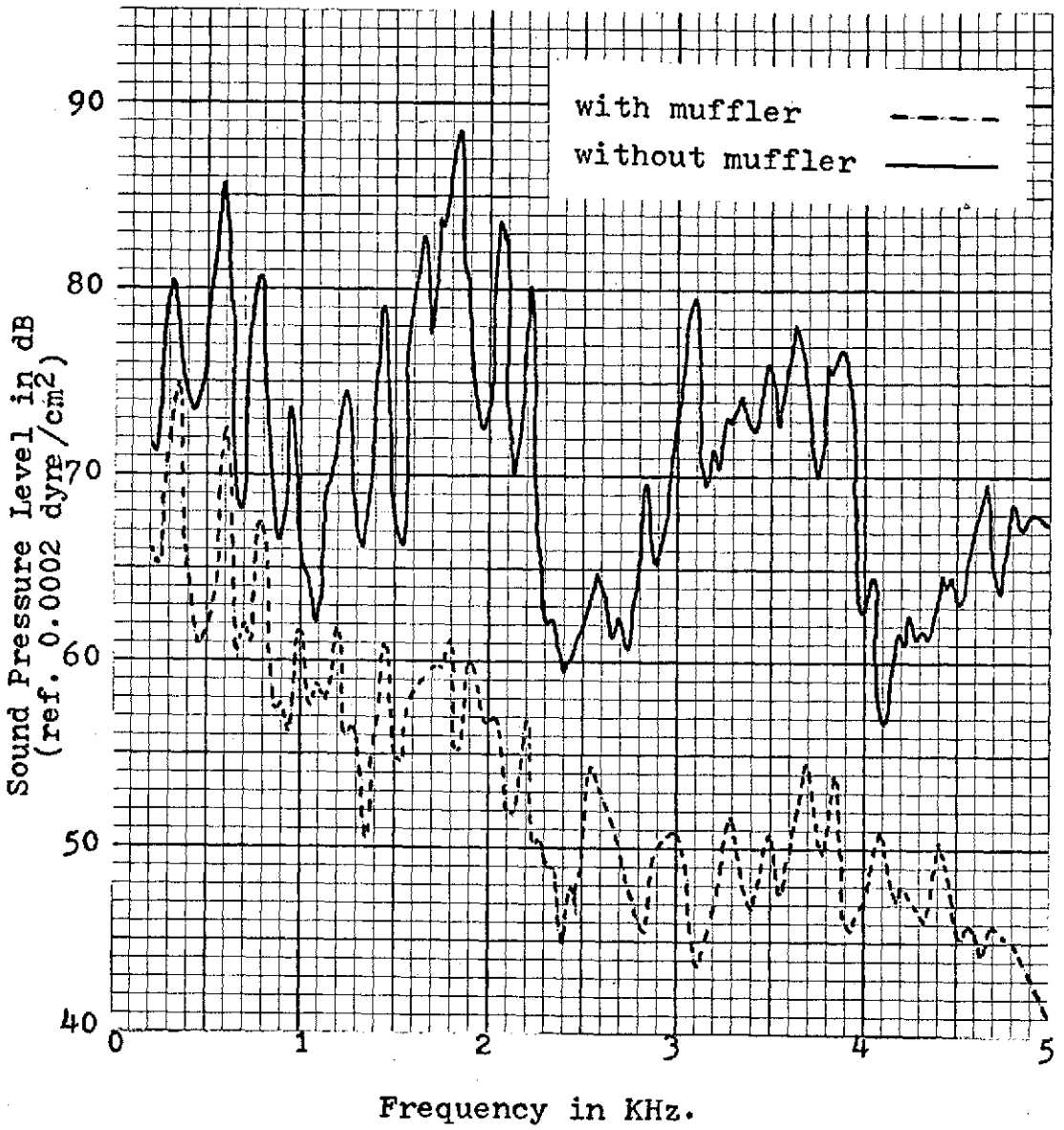

Figure 5-D. Spectrum analysis of far field radiated sound for 10.2 cm diameter model jet with and without muffler. (Band width: 50 Hz.)

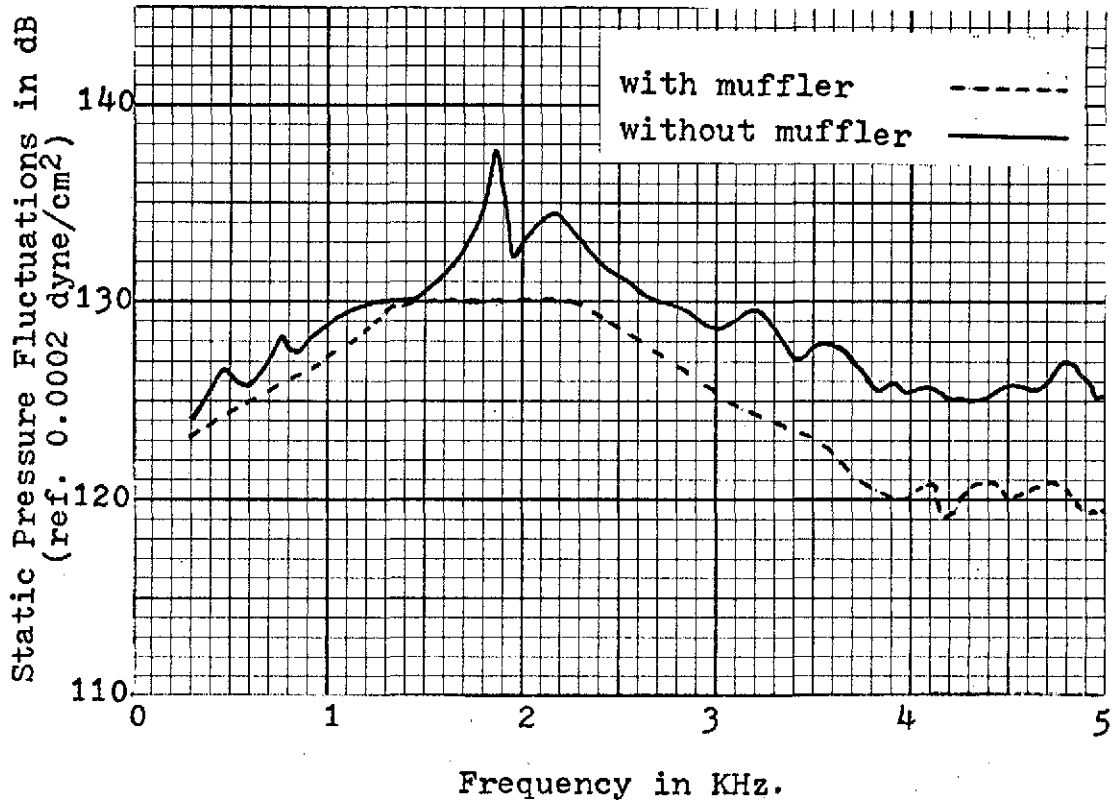

Figure 6-D . Frequency spectrum for static pressure fluctuations of model jet running at Mach .63 with and without muffler. Constant bandwidth: 50 Hz.
(probe position: X/D = 5.0 & Y/D = 0.0)

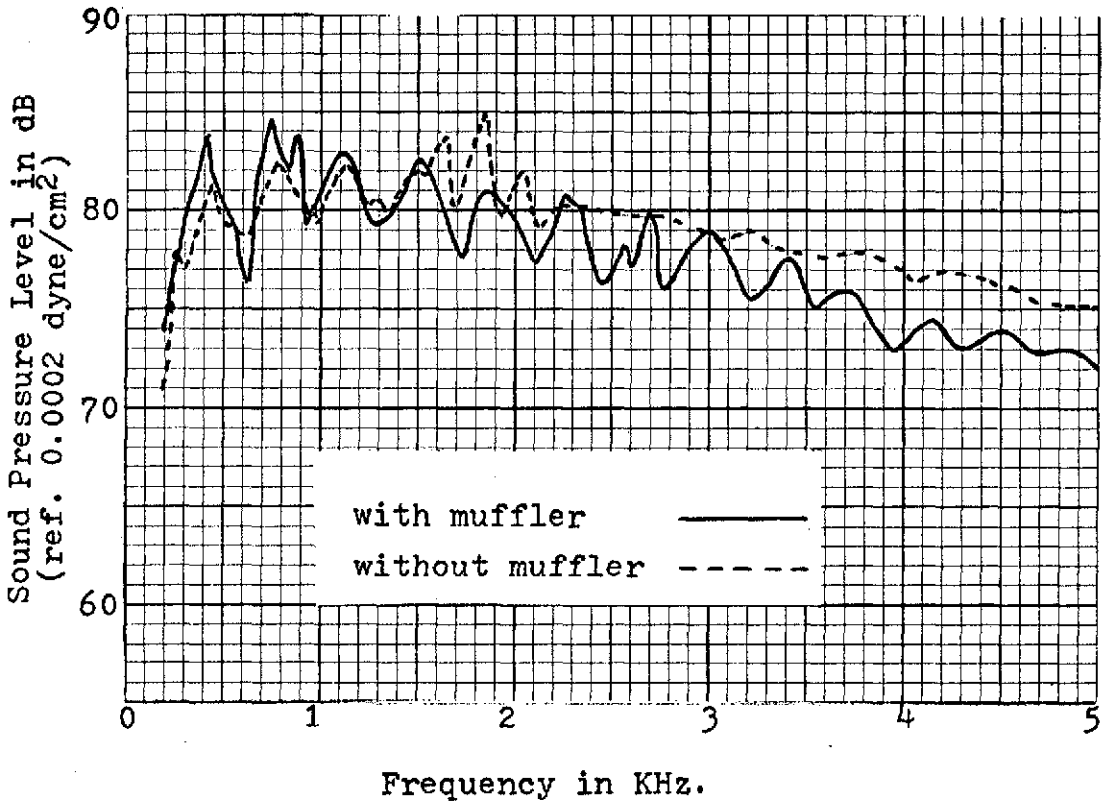

Figure 7-D. Spectrum analysis of far field radiated sound for model jet running at Mach .63 with and without muffler. (microphone position: $|\underline{x}| = 1.5$ m. and $\theta = 30^{\circ}$) (constant bandwidth: 50 Hz.)

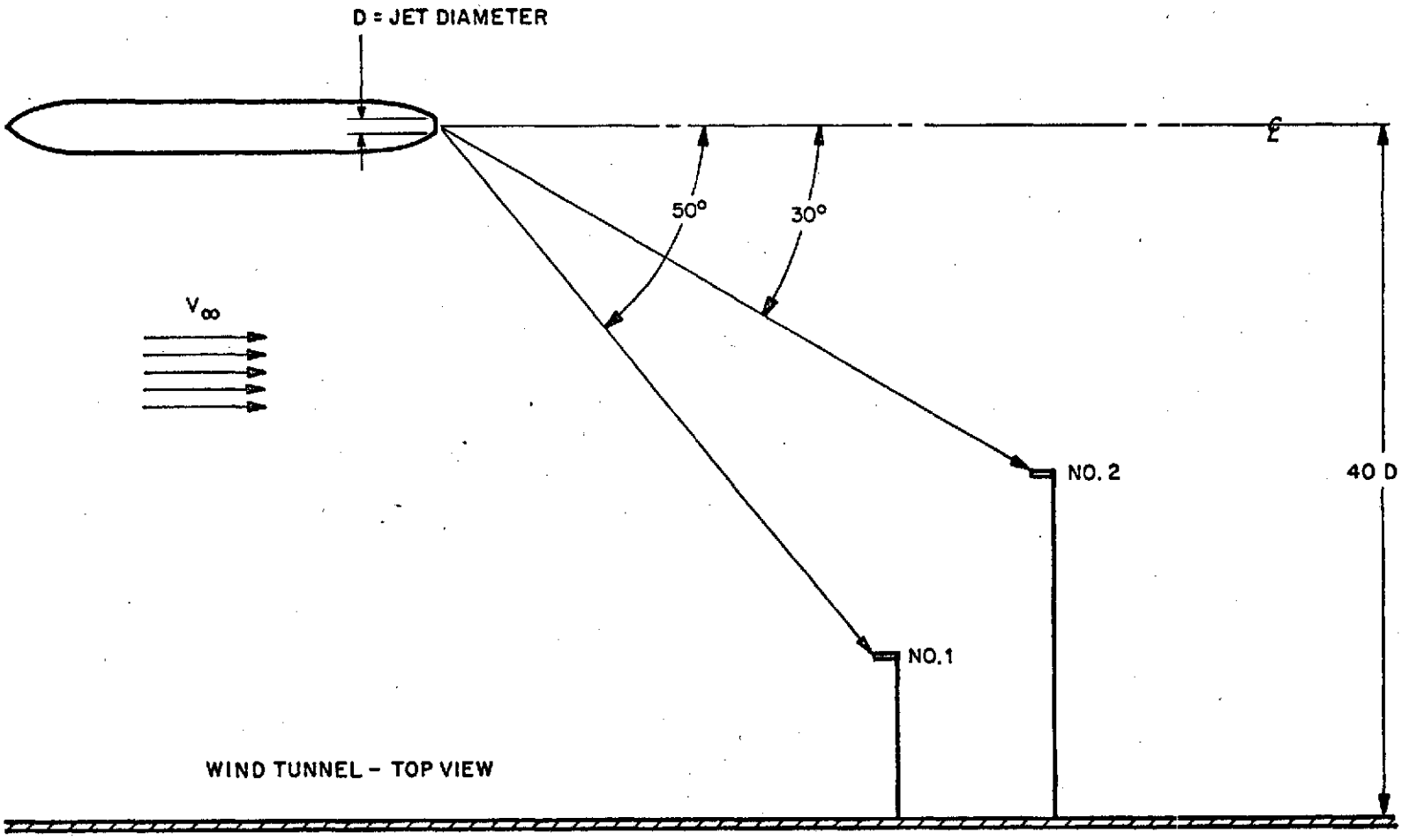

Figure 1-E. Test Geometry for Parallel Jet.

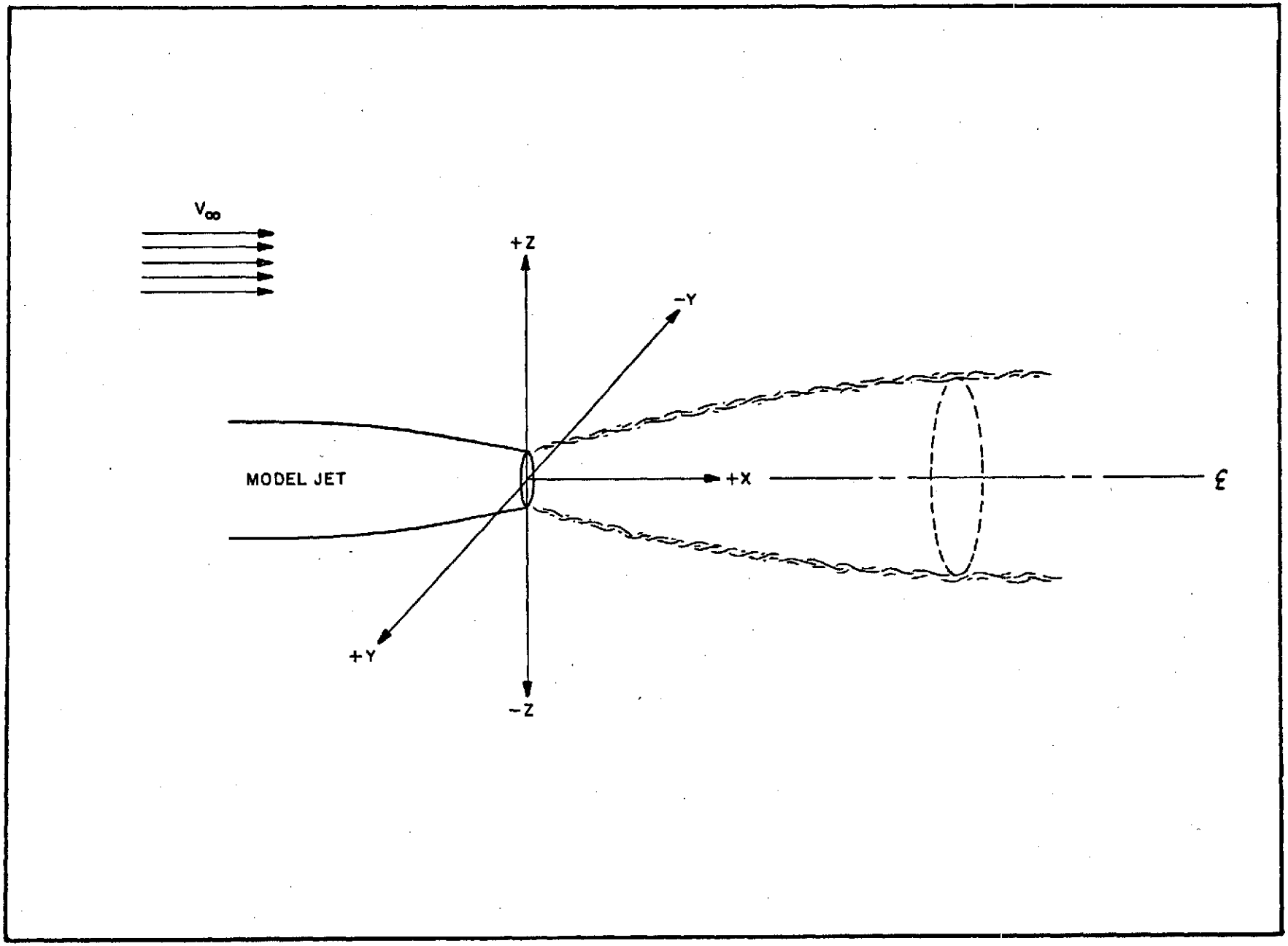

Figure 2-E. Pressure Probe Coordinate System for Parallel Jet.

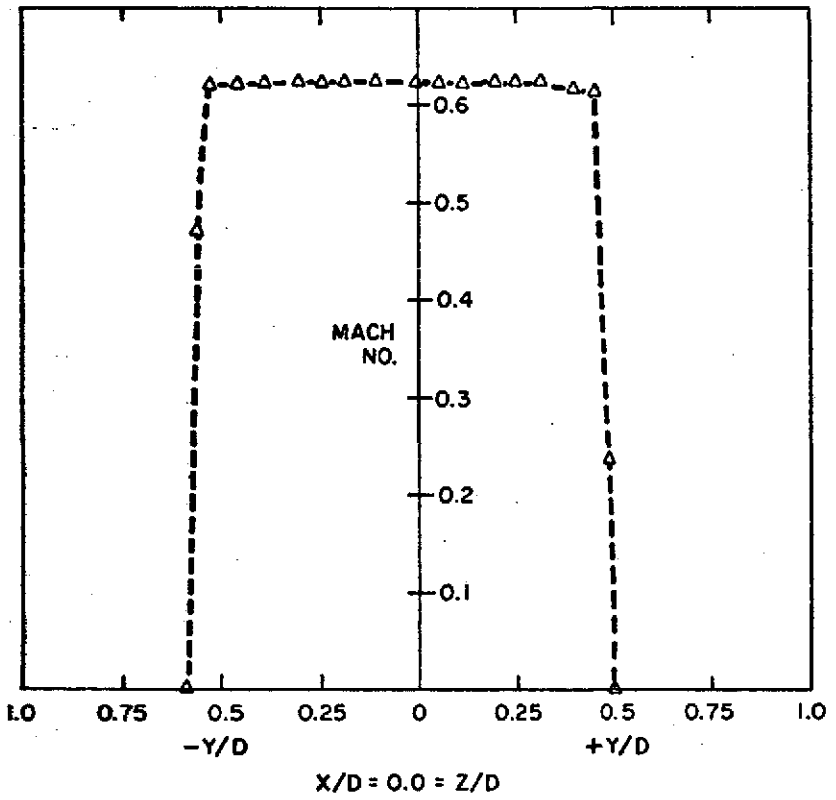

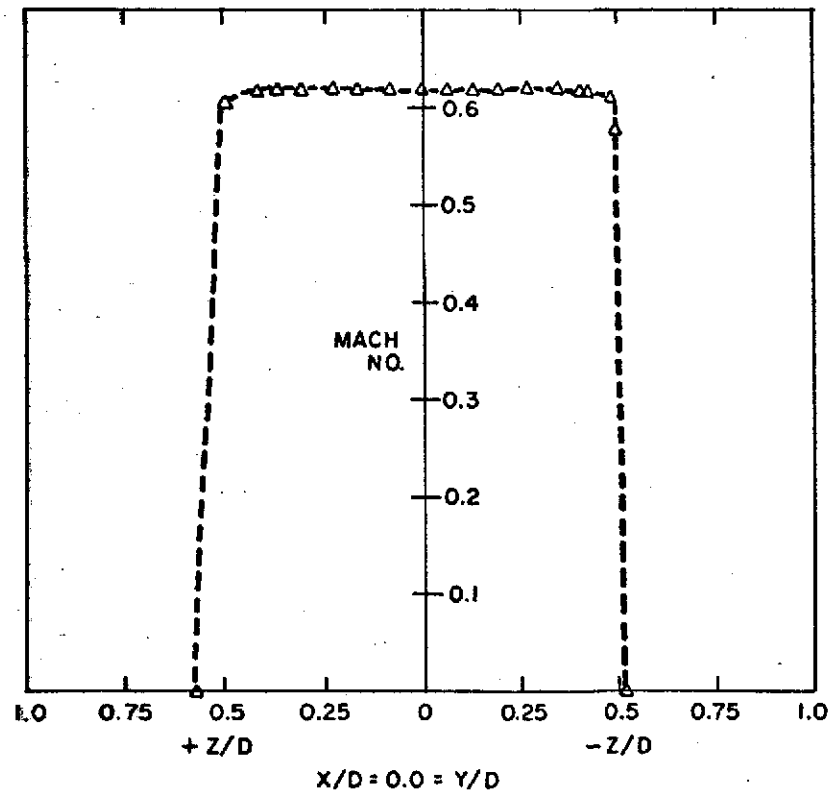

Figure 3-E. Velocity Profiles for Parallel Jet.

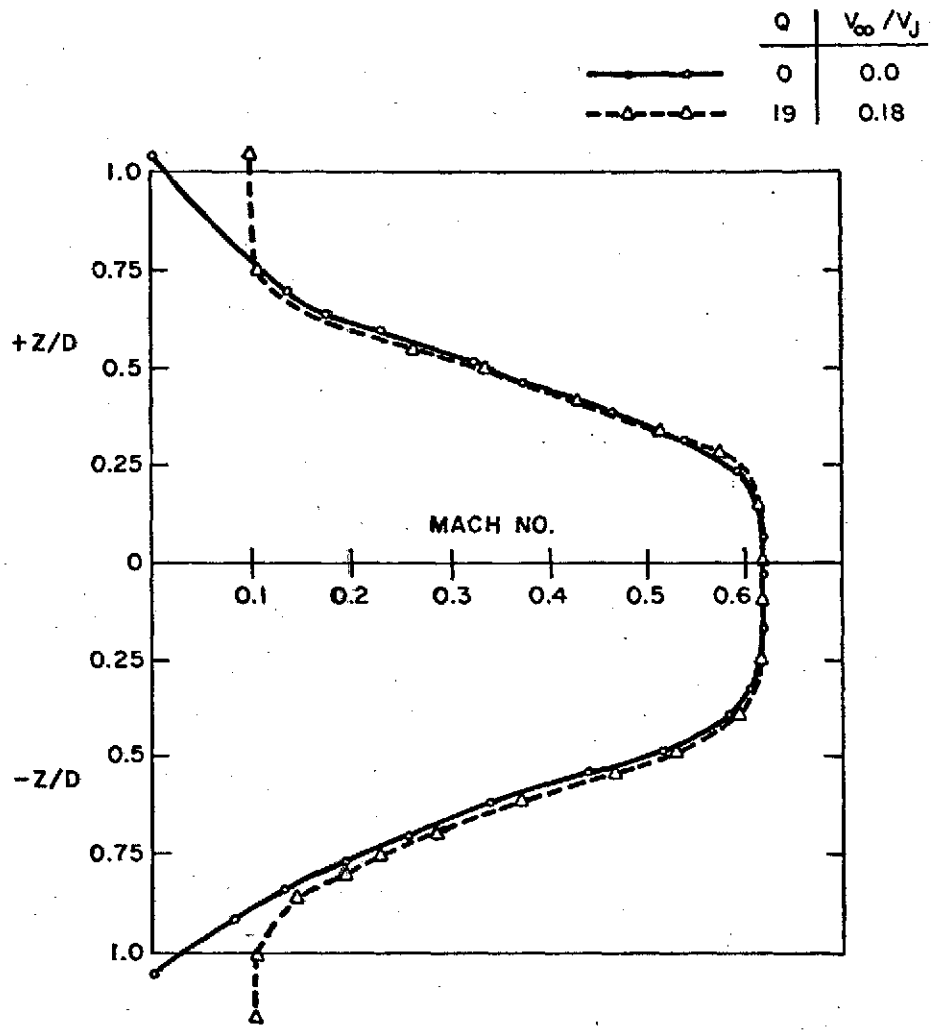

Figure 4-E. Velocity Profiles for Parallel Jet with Different Wind Tunnel Conditions.

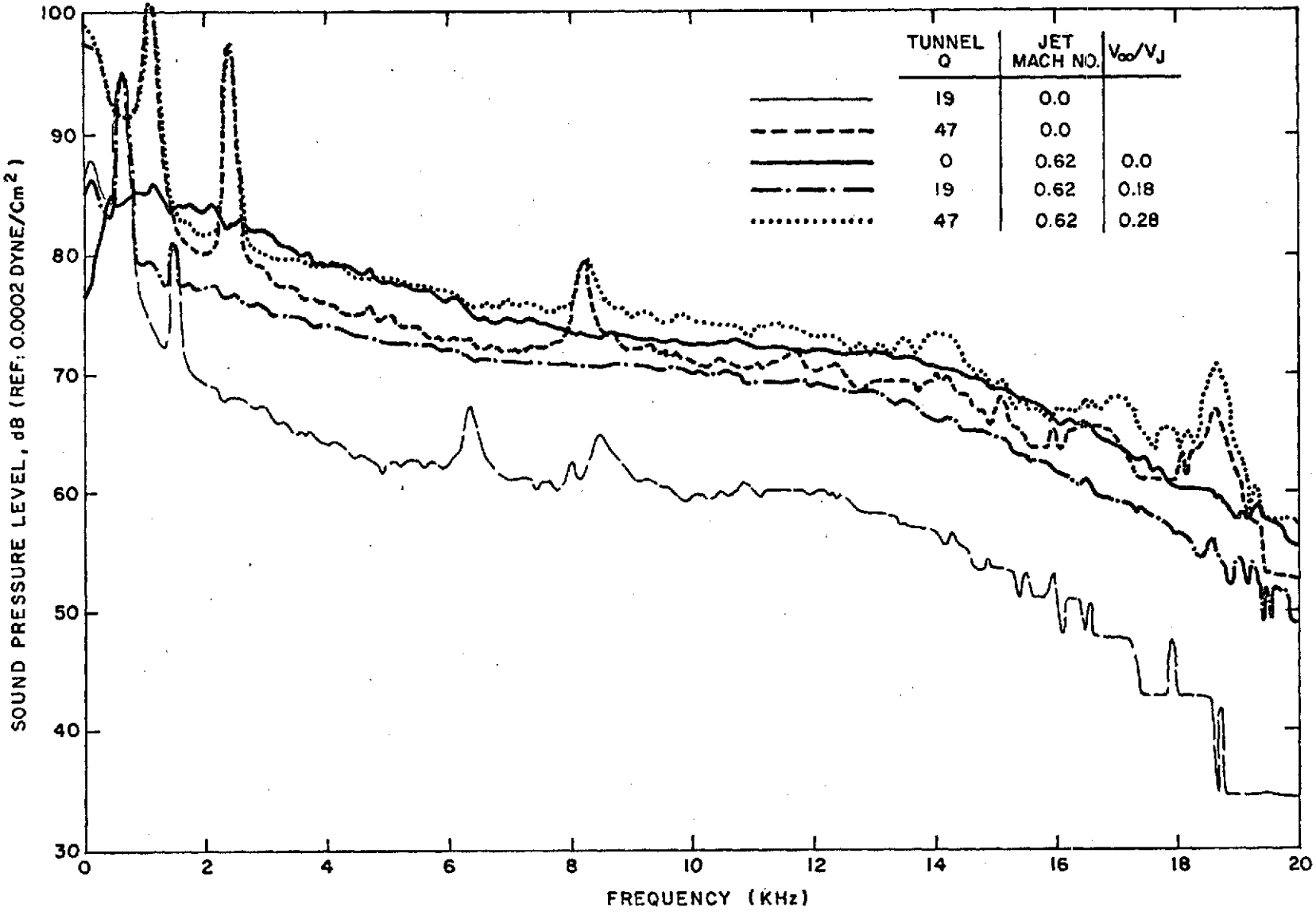

Figure 5-E. Narrow Band (50 Hz.) Frequency Spectra for Parallel Jet. (Far Field Position #2)

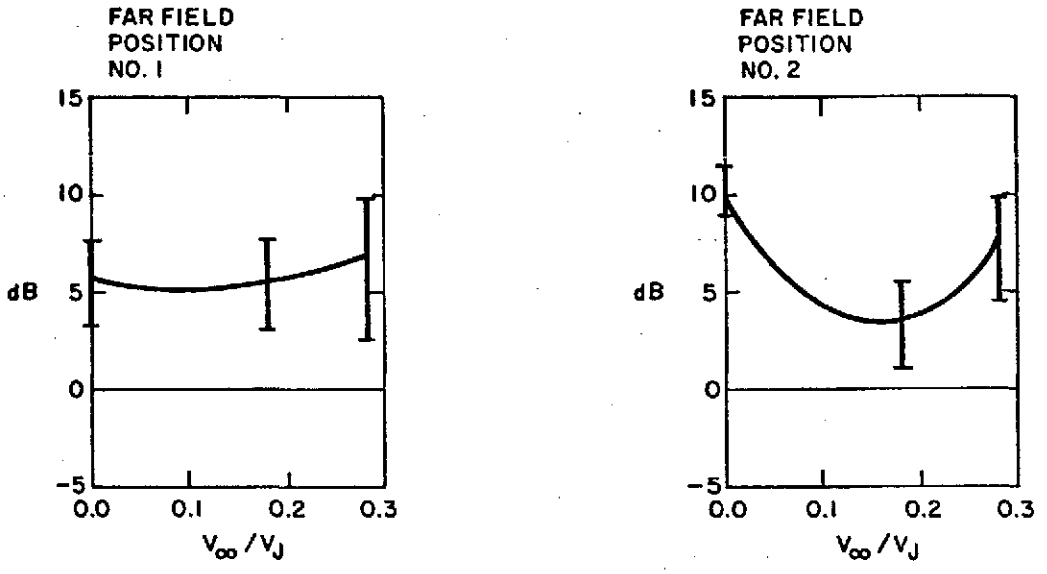

PROBE POSITIONS : X/D = 5.5 , Y/D = +0.3 , Z/D = 0.0

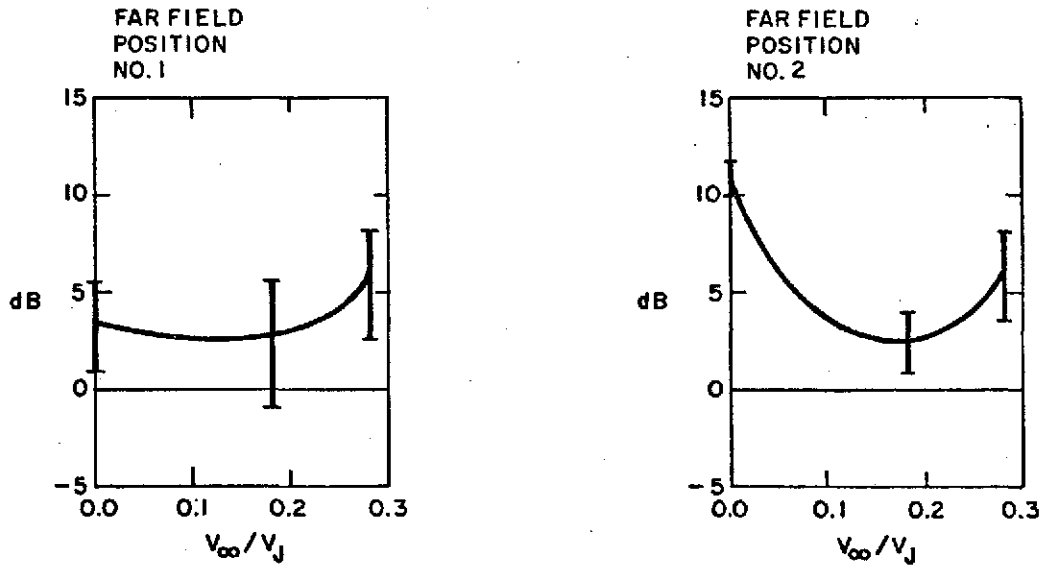

PROBE POSITIONS : X/D = 5.5 , Y/D = −0.13 , Z/D = 0.0

Figure 6-E. Effect of Tunnel Speed Variate on the Sound Radiated from the Eddy at the Probe Position for Parallel Jet.

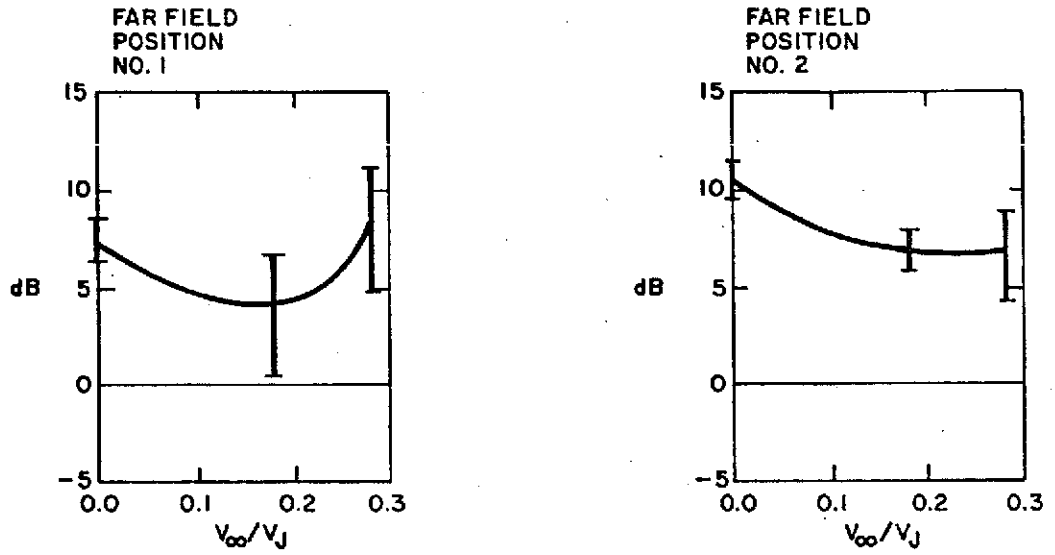

PROBE POSITIONS: X/D = 5.5, Y/D = 0.0, Z/D = -0.3

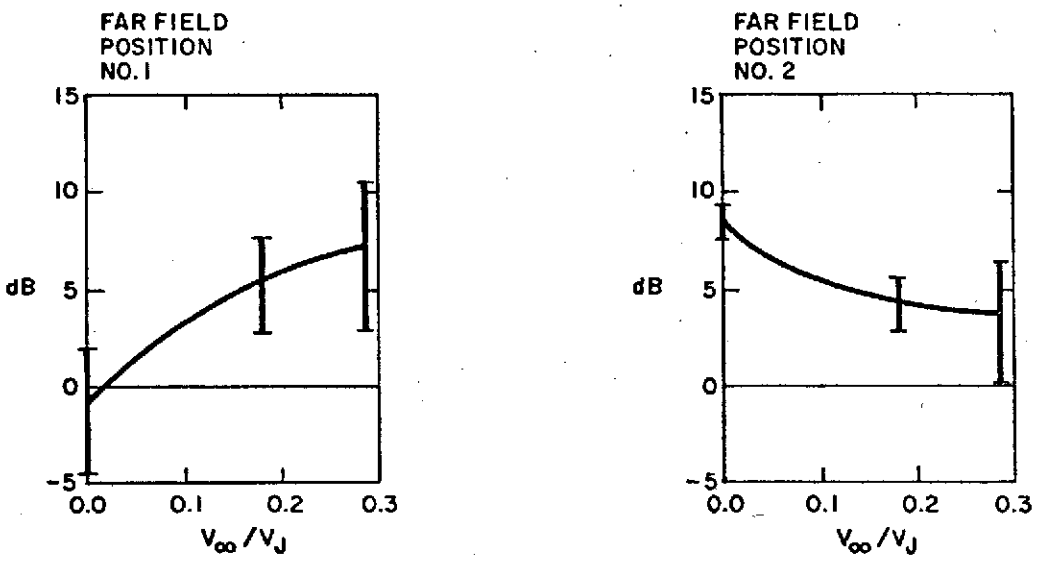

PROBE POSITIONS: X/D = 7.5, Y/D = Z/D = 0.0

Figure 7-E. Effect of Tunnel Speed Variate on the Sound Radiated from the Eddy at the Probe Position for Parallel Jet.

APPENDIX A. REMARKS ON THE CONSTANT C IN EQ. (5).

Begin by squaring (5); then substitute from (1) in (3) and in (the square of) (5) to find

$$\frac{1}{C} = \frac{|\langle \ddot{P}_o P_o \rangle|}{\ddot{P}_o' P_o'} \tag{A1}$$

where we assume for the correlation in (5) that the maximum value occurs for $\tau = 0$. We suppose that the various correlation volumes are approximately equal. The process p_o is statistically stationary so we find $\langle \ddot{P}_o P_o \rangle = -\langle \dot{P}_o^2 \rangle$ and (A1) can be written

$$C = \frac{P_o' \ddot{P}_o'}{\dot{P}_o'^2} \tag{A2}$$

By differentiating p_o it would appear that (A2) would yield a simple method to determine C. Unfortunately the static pressure has errors in it at higher frequency. Two which can be named are the following. First, the fact that turbulent flow is being convected past the probe means that part of the time variation in p_o is due to this convection: That part of the time variation would not be observed in a system moving with the mean flow--what is really desired for (1) (see discussion after (1)). Secondly for the higher frequency portions of p_o there is some reason to believe that the propagating sound is an important contributing element. As described in the theory section (and in associated references) p_o should be that portion of the static pressure which is 'hydrodynamic', i.e., which would occur if the fluid were truly incompressible. For the important frequency components in p_o there is no difficulty on this question. The difficulties just described do not in general permit a sensible determination of the RMS values of derivatives, such as those required for the expression (A2). It is hoped that in the future these difficulties can be overcome.

APPENDIX B. ELIMINATION OF REVERBERANT EFFECTS, FROM NORMALIZED CORRELATIONS.

The 7'x10' wind tunnel acts like a semi-reverberant chamber and therefore it is necessary to use a correction factor in order to simulate an experiment being conducted in a free field environment. In particular when normalizing the cross correlations the effects of reflections (and other non-correlated noises) enter into the normalization process.

In the present experiment we are concerned with calculating the normalized cross-correlation between the output of the static-pressure probe microphone and that of the far field microphone. Recall that a prime represents an RMS value. Use the standard definition of a normalized correlation,

$$c(r,\tau) = \frac{\langle p_o p \rangle}{p_o' p'} \qquad (B1)$$

where p_o is the pressure signal seen at the probe microphone and p is the signal sensed at a particular far field position. Here r is the distance from the probe to the far field position and τ is the time delay in the correlation. When operating in the 7'x10' wind tunnel p consists of not only the direct signal from the source but also the reverberant field, those signals which initially were propagated in different directions but due to reflections were sensed at the far field microphone position. In addition p contains the tunnel background noise. We have

$$p = p_{oo} + p_{o1} + p_{o2} + \cdots + p_{oN} + p_{oH.O.} + p_n \qquad (B2)$$

where p_{oo} is the pressure due to the direct signal and the other terms p_{o1}, p_{o2} etc. are the various reflections, numbered chronologically. For higher order reflections, the reflections in the correlations are no longer discrete and of course become smaller and lost in the noise; we lump those signals together and call their sum $p_{oH.O.}$. The uncorrelated (with the jet noise) background noise, including local noise effects caused by turbulence

at the microphone, is called p_N. Using (B2), (B1) can be written

$$\frac{\langle P_o P \rangle}{P_o' P'} = \left(\langle P_o P_{oo} \rangle + \langle P_o P_{o1} \rangle + \ldots + \langle P_o P_{on} \rangle + \langle P_o P_{o\,H.O.} \rangle \right) \Big/ P_o' P' \qquad \text{(B3)}$$

recalling that p_o and p_N are independent. So we should observe n+1 peaks with n the number of separately discernible reflections. For p' use (B2), square and average,

$$P'^2 = P_{oo}'^2 + P_{o1}'^2 + \ldots + P_{on}'^2 + P_{o\,H.O.}'^2 + P_N'^2 \qquad \text{(B4)}$$
$$+ \text{cross terms}$$

All cross terms like

$$\langle P_{o1} P_N \rangle \qquad \text{(B5)}$$

vanish because the tunnel background noise is statistically independent of the jet noise. Further the first n reflections contained in the correlation are by hypothesis separated from one another so their cross terms vanish: Hence all the cross terms in (B4) vanish.

Now we look at a particular time dealy (τ) in the cross-correlation process, for example that time τ equal to the time required for the signal to propagate directly from the probe microphone to the far field microphone. All of the cross-correlations represented in (B3) vanish except one and we have, using (B4) and neglecting cross terms,

$$c(r,\tau) = \langle P_o P_{oo} \rangle \Big/ \left(P_{oo}'^2 + \ldots + P_{on}'^2 + P_{o\,H.O.}'^2 + P_N'^2 \right)^{1/2} P_o' \qquad \text{(B6)}$$

If the same experiment were being conducted in a free field environment, e.g. an anechoic room, the "correct" normalized cross-correlation function, c_c would be

$$c_c(r,\tau) = \langle P_o P_{oo} \rangle \Big/ P_o' P_{oo}' \qquad \text{(B7)}$$

We must multiply (B6) by a correction factor, K, in order to obtain (B7). Before doing this we examine the higher order reflection terms and the effects of acoustic losses.

To calculate K we use source images in the tunnel walls to replace reflections. The mean square sum of relfections is

$$\bar{D} \sum_{m=1}^{\infty} P_{oo}'^2 \; r_{oo}^2 / r_{om}^2 \; e^{-\bar{a} r_{om}} / \tfrac{1}{2}(A+B) \qquad \text{(B8)}$$

where

r_{oo}= distance from real source to far field microphone.

r_{0m}= distance from image source to far field microphone.

$\bar{D}$ = average source directivity constant (would be equal to one for a true simple source).

A&B= cross-sectional dimensions of wind tunnel.

$\bar{\alpha}$ = average absorption coefficient of wind tunnel walls for the acoustic reflections.

Expanding the summation and dividing (B8) by p_{oo}, we have

$$p'^2_{o1}/p'^2_{oo} + p'^2_{o2}/p'^2_{oo} + \ldots + p'^2_{on}/p'^2_{oo} + \bar{D}\,2\pi\,\frac{r_{oo}^2}{AB}\,E\left(\frac{\bar{\alpha}\,a_o T_n}{\tfrac{1}{2}(A+B)}\right) \qquad (B9)$$

where E is an exponential integral,

$$E\left(\frac{\bar{\alpha}\,a_o T_n}{\tfrac{1}{2}(A+B)}\right) = \int_{\frac{\bar{\alpha}\,a_o T_n}{\frac{1}{2}(A+B)}}^{\infty} \frac{dX}{X}\; e^{-X} \qquad (B10)$$

The ambient speed of sound is defined as a_o and T_n is the time delay required for the signal from the furthest image (reflection) which can be identified in the cross-correlation data. Therefore $a_o T_n$ is the distance from that image source to the far field microphone. The integral approximates the effects of the signals from the image sources which are not clearly identifiable in the cross-correlation data. Therefore the correction factor to be applied to (B6) to obtain (B7) is

$$K=\left[1 + \frac{p'^2_{o1}}{p'^2_{oo}} + \ldots + \frac{p'^2_{on}}{p'^2_{oo}} + \bar{D}\,2\pi\,\frac{r_{oo}^2}{AB}\;E\left(\bar{\alpha}\,a_o T_n/\tfrac{1}{2}(A+B)\right) + \frac{p'^2_N}{p'^2_{oo}}\right]^{1/2} \qquad (B11)$$

The values p'_{on}/p'_{oo} for the image sources which are identifiable from the cross-correlation data can be approximated by the ratio of the values of the cross-correlations (normalized) of the particular peaks.

The average source directivity constant is calculated from the anechoic source directivity if available; if not it must be estimated from other data.

$$\bar{D} = \tfrac{1}{4}\pi \int_0^{2\pi}\int_0^{\pi} \frac{P_{oo}(\theta,\phi)}{P'^2_{oo}(0,0)}\;\sin\theta\;d\theta\;d\phi \qquad (B12)$$

The average absorption coefficient $\bar{\alpha}$ used in the calculation of K was

.02, obtained from measurements of reflection losses as reported in standard references.

Using this correction technique a number of cross-correlation measurements made in the 7'x10' wind tunnel were corrected; the tunnel was off so $p'_n = 0$. The results of this correction process are shown in Table I-D, where the corrected values for the wind tunnel measurements are compared to similar measurements made in an anechoic chamber. The results show good agreement for the two sets of measurements, except for the case of microphone #1 when the source is canted. In this orientation the source is pointing directly at microphone #1.

In actual applications the wind tunnel would of course be operating so that one would have to determine p'_N; this is easily done by operating the wind tunnel without the jet and taking the sound levels. This pressure level is then used in (B11).

The successful use of this method depends upon having a sufficient number of reflection components in the cross-correlations so that the integral approximation for the higher order terms (those called $p_{oH.O.}$ here) is valid. In our work with the wind tunnel, we could not process the data for a sufficient period of time so that was the case. It is expected that in other applications it would be a possibility.

APPENDIX C. SOUND SOURCE MEASUREMENTS IN ANECHOIC CHAMBER AND WIND TUNNEL

In order to study the influence of the 7'x10' wind tunnel reflections surfaces on cross-correlation functions initial, measurements were made using a sound source (Altec 802D driver). The measurements were first made in an anechoic chamber and then repeated in the 7'x10' tunnel.

A test was used consisting of a source with four far field microphones in different directions. In addition a probe-type microphone was positioned approximately 26.7 cm from the source. The sound source was driven by a white noise generator.

Two basic experiments were conducted: one, the sound source in a vertical orientation, and two, the source slanted toward one of the far field microphones. The slanting was intended to give directional effects. The outputs of the far field microphones and the probe microphones and the probe microphone were recorded.

Auto correlations and cross-correlations of the recorded signals were made. The main interest centered on the cross-correlation between the probe (near field) microphone signal and the various far field microphones. In the anechoic chamber the normalized cross-correlations between the probe microphone and the different far field microphones varied between 0.82 and 0.89.

When the experiment was rerun in the 7'x10' wind tunnel a significant degradation of the normalized cross-correlation values occurred, the values varying between 0.41 and 0.59.

Our first cross-correlation ideas, as described in Appendix B, treated the normalized cross-correlation functions calculated for the wind tunnel data in such a way that the results would approximate a

free field condition. As a step in calculating this formula, it was necessary to measure the directivity pattern of the sound source (Altex 802D driver). This directivity pattern, measured in anechoic chamber, is shown in Fig. 1-C.

Employing the data from the directivity pattern and using an average absorption coefficient 0.02 for the wind tunnel walls, a number of cross-correlations made in the 7'x10' wind tunnel were corrected. The results of this correction process is shown in Table 1-C, where the corrected values for the wind tunnel measurements are compared to similar measurements made in an anechoic chamber. The results show good agreement for the two sets of measurements, except for the case of microphone #1 when the source is canted. In this orientation the source points directly at the microphone.

In addition to the cross-correlation measurements, frequency spectra of the far field signals were made for both the anechoic chamber and wind tunnel tests. Fig. 2-C shows the results of such measurements. For this particular plot the far field microphone was located approximately 1.3 meter from the source and at an angle of 40^{o} from the source axis. In the wind tunnel this microphone was located in front of one of the side walls. These spectra were made with a constant bandwidth of 50 Hz. As expected, due to reflections, the signal inside the tunnel shows high amplitude and a larger number of irregularities.

APPENDIX D. MUFFLER FOR MODEL JET

One of the preliminary tests conducted during the course of this program was made to insure that the sound generated by the model jet was true aerodynamic noise and not noise originating in valves, etc., upstream from the jet nozzle exit. This test consisted of replacing the 3.8 cm. diameter jet nozzle with a 10.2 cm. diameter pipe with all controls kept constant to approximate equal mass flow.

Far field sound measurements were recorded and analyzed for both conditions. Fig. 1-D shows the spectra of the far field microphone signals with the microphone located at an angle of 30° and a distance of 1.5 m from the jet. The dominant peak in the vicinity of 1850 Hz, clearly results from a noise mechanism located upstream from the jet exit (such as valve noise). The same peak was evident in a spectrum made for a static pressure fluctuation probe inserted in the jet wake.

It was decided that an acoustic muffler would be designed and built prior to any further testing. This muffler, shown in Fig. 2-D is a reactive - dissipative device with an effective length of approximately 4.4 meters. It has an input and output area ratio of 5.44. It includes two right angle bends. The inner portion of the muffler consists of a perforated pipe with a 44.4% opening. This pipe is covered with a 10.2 cm. thick foam blanket. The random signal absorption for this foam is shown in Fig. 3-D.

With this acoustic muffler inserted in the system, the above test was repeated. Fig. 4-D shows the result for the muffler, for 3.8 cm. and 10.2cm diameter jets. These curves show that the muffler provides considerable attenuation for 900 Hz and above. As expected, due to the dimensions of the muffler the attenuation below 600 Hz becomes small (but of course is not needed).

The spectra for the far field sound for the 10.2 cm. diameter nozzle with and without muffler are shown in Fig. 5-D. Considerable attenuation is evident, in particular at 1850 Hz. where the attenuation is approximately 33 dB: the dimensions for the right angle bends were chosen to give maximum attenuation for this frequency.

The spectra for the static pressure fluctuation and the far field radiated sound for the 3.8 cm. diameter jet running at Mach 0.63 with and without the acoustic muffler are shown in Figs. 6-D and 7-D respectively. For both cases the muffler has eliminated the peak at 1850 Hz.

In addition to the narrow band spectra, cross-correlations and autocorrelations were made. In all cases the periodicity in the functions which was present when similar measurements were made before the acoustic muffler was installed, no longer appeared. The cross-correlations between the pressure probe and the far field microphones resembled those functions measured in an anechoic chamber with the addition of reflected pulses as expected.

APPENDIX E. PARALLEL JET

The main purpose of this portion of the study was to use the results as a reference for the interpretation of the results of the perpendicular jet experiment. It was anticipated that the parallel jet experiment would be an intermediate step between a model jet in an anechoic chamber (about which much information is available)[11] and a model jet oriented normal to the flow, in a wind tunnel. Due to experimental problems the results were not as helpful as had been hoped.

E.1 Experiment

The parallel jet experiment employed a model jet aligned parallel to the wind tunnel flow. A diagram of the test configuration is shown in Fig. 1-E.

The model was a circular jet with a 3.8 cm. diameter. In order to insure that the noise generated by this jet was aerodynamic noise (to eliminate upstream noise in the air supply) it was necessary to design and install a dissipative-reactive muffler with an effective length of 4.4 meters ahead of the jet exit. The design and the acoustic properties of this muffler are described in Appendix D of this report. The jet was positioned so that its centerline coincided with the centerline of the wind tunnel.

Two far field microphones were employed. These transducers were at positions 1.5 meters (40 jet diameters) from the jet exit at 30° and 50°, measured from the centerline. They were attached to the side wall of the wind tunnel at the same height as the jet centerline and used B&K 1.3 cm. condenser microphones, with nose cones, as active elements. In addition a pressure probe (a 0.32 cm. microphone of the same type) was employed to measure and record the static pressure fluctuations within the turbulent volume.*

*Errors made, when measuring static pressures in this way, have been discussed previously[4-7]. For the most part such errors are not important here.

The coordinate system defined for this pressure probe, for this experiment is shown in Fig. 2-E.

All hardware employed inside the 7'x10' wind tunnel was designed and constructed to minimize noise generation arising from the tunnel flow interaction.

The basic experiment consisted of running the model jet at a Mach number of 0.62 and varying the wind tunnel conditions. Three different conditions were used in the wind tunnel. They were:

a. Static case--no flow--Q (dynamic pressure) = 0, resulting in a velocity ratio of zero.

b. Q = 19, flow speed approximately 38.4 m/sec giving a velocity ratio of 0.18.

c. Q = 47, flow speed approximately 60.4 m/sec giving a velocity ratio of 0.28.

The velocity profiles at the jet exit for both the Y and Z axes for the model jet running at Mach 0.62 with the wind tunnel in a static condition (no flow) are shown in Fig. 3-E. These profiles show the typical "top hat" characteristics, with good symmetry for both axes.

With the wind tunnel running with a Q of 19 a velocity profile along the Z axis, was made at X/D equal 3 and Y/D equal zero. This profile and the exact profile for the wind tunnel in a static (Q=0) condition are shown in Fig. 4-E. The tunnel flow seems to have little effect on the velocity profile except of course near the skirts where the velocity does not reach zero as in the static case but rather approaches the velocity of the tunnel flow. This perhaps surprising lack of effect internal to the jet is noteworthy.

The experiment consisted of recording the fluctuations at seven pressure probe positions and at the two far field microphones, for test conditions previously described.

E.2 Analysis

The data analyses consisted of doing narrow band (50 Hz) frequency analyses of the signals recorded, and calculating the cross-correlation functions for the various probe positions and for the two far field microphones. A block diagram of the electronic equipment used in the data analysis is shown in Fig. 6 of the report.

E.2.1 Frequency Analyses

Narrow band (50 Hz) frequency spectrums were made of the pressure signals. The frequency spectrums for the far field microphone position #2 are shown in Fig. 5-E. For the tunnel running with a Q of 19 and of 47, the background noise (tunnel noise) shows two dominant peaks, each with their first harmonics. The main peak for Q equals 19 is located at approximately 750 Hz while the main peak for Q equals 47 has a frequency of approximately 1200 Hz. The ratio between these two frequencies is 1.6 which turns out to be the ratio of the tunnel velocities for the wind tunnel operating at a Q of 19 and 47. Since these frequencies are much too high for the fan noise generated by the wind tunnel drive mechanism, it is believed that these peaks are generated by some type of a whistle created by the flow interaction with some artifact in the tunnel (e.g. hole, strut, etc.).

The aerodynamic noise generated by the model jet is typically 10 to 15 dB higher than the tunnel noise for Q equal 19, except at the fundamental peak which rises 10 db above the jet noise. For the tunnel running at a Q of 47, the difference is more like 2 or 3 dB with the peak frequency and its first harmonic being about 15 dB above the jet noise. To sum up, for the higher tunnel speed there is difficulty with tunnel noise; correlation methods are needed (and are used).

E.2.2 Cross-Correlation measurements

As described in the theory section of this report the raw cross-correlates between the far field microphones and the static pressure probe, at various positions, were measured. The (maximum) measured cross-correlation, times the square of the distance from the pressure probe to the far field microphone, and divided by the RMS value of the static pressure fluctuations are plotted against the velocity ratio (V_{oo}/V_j) in Fig. 6E and 7E. Such a plot, see Section 2, shows the effect of tunnel speed variation upon the sound radiated from the eddy at the probe position. The dB values are referenced to an arbitrary number and are to be used to give relative values for different positions or different speeds. It should be understood that the curves are rough approximations since they are derived from only three points (velocity ratios of 0, 0.18, and 0.28). The error flags on these curves are calculated from the noise seen on the cross-correlation functions. Since a finite averaging time is employed in the calculation of the cross-correlation functions there exists a noise fluctuation (see Section 2) which gives rise to an uncertainty in the true value, the lower the amplitude of the function the higher the uncertainty. This is especially noticeable in the curves for microphone #2 where the errors increase as the background noise of the tunnel increases.

From work done previously on a model jet in the anechoic chamber, the eddies in the vicinity of the probe positions, for the various curves shown in these two figures, are known to be strong noise radiators for smaller far field angles (microphones #2). For larger far field angles (microphone #1) the shear region is also a very active noise-radiating region. Probes were placed in the shear region but (possibly due to a large mechanical vibration experienced by the probe, over a frequency region of 2200 to 3800 Hz) the data could not be analyzed. This noise, which appeared on all the recordings for the parallel jet experiment, required the use of a band

rejectifilter in the determination of the cross-correlation functions. This significantly contributed to the errors since it tended to reduce the true value of the cross-correlation function especially for the higher far field angles (microphone #1) where the sound field shows higher frequency content that at the lower angles. Taking these two factors into consideration plus the fact that the tunnel noise is more important at microphone #1, as previously stated, it is undertandable that the error flags are so large for this position--even for a velocity ratio of zero. The large errors for curves for far field position #1 (in Fig. 6E and 7E) make interpretation difficult. It is noted that in Fig. 6E the probe is located just off the jet axis (Y/D = +0.3 and -0.13), 5.5 diameters from the jet exit. These two positions are in the same plane as the far field microphones and the jet centerline (X-Y Plane). For Y/D equal -0.13 the sound generated at this position and experienced at the far field position #2 is reduced from 6 to 11 dB (limits of the error flags) when the velocity ratio goes from zero to 0.18. As the velocity ratio is further increased the reduction lies between 2 to 8 dB. Whether a minimum actually occurs at V_{oo}/V_j equal 0.18 cannot be accurately determined from the curve due to the relatively large error flags and to the fact that only three velocity-ratio points were measured. For Y/D equal + 0.3 the results are very similar to those just described. For far field microphone position #1 no trend can be inferred from the curves for the reasons just mentioned.

The top curves in Fig. 7E represent the results for the static pressure probe located at X/D equal 5.5 and Z/D equal -0.3: The probe is located in the X-Z plane. Increasing the velocity ratio from zero to 0.18 results in a sound reduction of 2 to 5.5 dB at far field position #2. As the velocity ratio is further increased the errors are too large to determine the effect. Therefore, no definite trend can be stated when the velocity increases from 0.18 to 0.28. For far field position #1 no definite trend

can be observed for the reasons just mentioned in connection with Fig. 6-E

The lower curves in Fig. 7-Ewere calculated for the pressure probe located on the jet axis (centerline), 7.5 diameters from the jet exit. For the far field position #2, an increase in the velocity ratio from zero to 0.18 results in a reduction from 2 to 6.5 dB. The effect of a further increase in the velocity ratio cannot be determined because of the error flags. Similar problems are met for position #1.